SOFTWARE IMPLEMENTATION OF KEY TRANSCEIVER ALGORITHMS FOR AN IN-BAND FULL-DUPLEX DVB-S2-BASED SATELLITE COMMUNICATION SYSTEM

A THESIS SUBMITTED TO

THE GRADUATE SCHOOL OF

ENGINEERING AND NATURAL SCIENCES

OF ISTANBUL MEDIPOL UNIVERSITY

IN PARTIAL FULFILLMENT OF THE REQUIREMENTS FOR

THE DEGREE OF

MASTER OF SCIENCE

IN

ELECTRICAL, ELECTRONICS ENGINEERING AND CYBER SYSTEMS

By

Khaled Walid Elgammal

January, 2021

SOFTWARE IMPLEMENTATION OF KEY TRANSCEIVER AL-
GORITHMS FOR AN IN-BAND FULL-DUPLEX DVB-S2-BASED
SATELLITE COMMUNICATION SYSTEM

By Khaled Walid Elgammal

January, 2021

We certify that we have read this thesis and that in our opinion it is fully adequate, in scope and in quality, as a thesis for the degree of Master of Science.

_____
Assoc. Prof. Dr. Mehmet Kemal Özdemir (Advisor)

_____
Prof. Dr. Hasari Çelebi

_____
Assist. Prof. Dr. Tunçer Baykaş

Approved by the Graduate School of Engineering and Natural Sciences:

_____
Assoc. Prof. Dr. Yasemin Yüksel Durmaz
Director of the Graduate School of Engineering and Natural Sciences

ii

Foreword

This thesis marks the final chapter of my master study in Electrical-Electronics Engineering and Cyber Systems program at Istanbul Medipol University.

In this thesis, a new Same-Frequency Full-Duplex algorithm is proposed and tested for satellite communication systems employing DVB-S2 standard. The proposed algorithm is able to reach a performance comparable to that of a Half-Duplex system.

This work wouldn't have seen the light without the precious guidance and support of my advisor, Assoc. Prof. Dr. Mehmet Kemal Özdemir. I would also like to send my gratitude to all of my classmates in IMU. Finally, I am thankful to my family which supported me during this journey.

I hereby declare that all information in this document has been obtained and presented in accordance with academic rules and ethical conduct. I also declare that, as required by these rules and conduct, I have fully cited and referenced all material and results that are not original to this work.

Name, Last Name: KHALED WALID ELGAMMAL

Signature   :

Acknowledgement

I would like to express my profound gratitude and thanks to my mentor and advisor, Assoc. Prof. Dr. Mehmet Kemal Özdemir for his continuous support and guidance during my study. He taught me much more beyond the subject of the thesis.

I thank my friends in Istanbul Medipol University for their help and fruitful discussions.

I deeply thank my parents and brothers for everything they have done for me, for their unconditional love and support.

Last but not least, I sincerely thank my wife for being in my life, for her patience and sacrifices.

Contents

List of Figures

List of Tables

List of Symbols

α_T Channel coefficient of transmitted signal echo at the SOI

S_T Transmitted message from the SOI to the satellite

Δd_T Time delay in the echo of the transmitted signal at the SOI

Δf_T Frequency offset in the echo of the transmitted signal at the SOI

$\Delta \Phi_T$ Phase offset in the echo of the transmitted signal at the SOI

α_R Channel coefficient of received signal at the site of interest

S_R Desired received message to the SOI

Δd_R Time delay of the desired received signal at the SOI

Δf_R Frequency offset of the desired received signal at the SOI

$\Delta \Phi_R$ Phase offset of the desired received signal at the SOI

s Number of slots in a DVB-S2 frame

G Linear block code to encode MODCOD and TYPE

I In-phase component

Q Quadrature component

r Received symbols

c SOF symbols

L SOF length

T_s Symbol rate

Δf_o Frequency offset

Φ_o Phase offset

R Cross-correlation of SOF with the received signal

$()^*$ Complex conjugate

N Frame length

R_{diff} Differential cross-correlation

z Beat signal

n AWGN

e Error

E_s/N_o signal-to-noise ratio

BW Bandwidth

dB Decibel

$\Delta\hat{f}$ Estimated frequency offset

M Auto-correlation length

R_l l-th pilot auto-correlation

$R_{M\&M}$ Mengali and Morelli auto-correlation

w Weight

L_p Pilot lentgth

arg Arguement

P Design parameter of Fitz frequency estimation method

$\Delta f_{o,max}$ uncertainty range of estimated frequency offset

Z Beat signal in frequency domain

$\hat{\Theta}_o$ Estimated phase offset

$\Delta\hat{f}_{ML}$ Estimated frequency offset using ML FFT

γ Step size

σ Noise standard deviation

a AWGN

A AWGN in wavelet domain

R_{sym} Received symbols in wavelet domain

$\hat{c}$ Estimator of c

C Received signal in wavelet domain

$\hat{C}$ C estimator

Δ Thresholding matrix

δ_i $i-th$ diagonal element of Δ

W Wavelet transformation matrix

W^{-1} Inverse wavelet transformation matrix

S Superimposed signal

STx_{echo} Transmitted signal component in superimposed signal

S_{Rx} Received signal component in superimposed signal

$\boldsymbol{\sigma_n}$ Noise standard deviation

$\boldsymbol{Tx}$ Ideal transmitted signal

$\boldsymbol{Rx}$ Ideal received signal

$\boldsymbol{\Delta f_{Tx}}$ Frequency offset of the transmitted signal

$\boldsymbol{\Delta f_{Rx}}$ Frequency offset of the received signal

$\boldsymbol{R_{Tx}}$ Cross-correlation of superimposed signal with the transmitted signal beyond the SOF

$\boldsymbol{L_{Tx}}$ Discrimination cross-correlation of the transmitted signal beyond + preamble length

$\boldsymbol{\Delta \hat{f}_{Tx}}$ Estimated frequency offset of the transmitted frame

$\boldsymbol{\Delta \hat{f}_{Tx,prior}}$ Prior Estimated frequency offset of the previous transmitted frame

$\boldsymbol{\hat{T}x_{echo}}$ Estimated echo of the transmitted signal

$\boldsymbol{\Delta \hat{f}_{Tx,ML}}$ ML estimated frequency offset of the transmitted signal

$\boldsymbol{Proj_B A}$ Projection of A onto B

$\boldsymbol{S_{Rx}}$ Received signal component in superimposed signal

$\boldsymbol{\Delta \hat{f}_{Rx,prior}}$ Prior Estimated frequency offset of the previous received frame

$\boldsymbol{\Delta \hat{f}_{Rx,ML}}$ ML estimated frequency offset of the received signal

$\boldsymbol{\Delta \hat{f}_{Rx}}$ Estimated frequency offset of the received signal

$\boldsymbol{S_{Rx,d}}$ Denoised received signal

$\boldsymbol{S_{Rx,d,\Delta \hat{f}_{Rx,prior}}}$ Denoised received signal compensated by prior frequency offset

$\boldsymbol{MSE(.)}$ Mean squared error

$\boldsymbol{S_{Rx,d,\Delta \hat{f}_{Rx,prior}+\Delta \hat{f}_{Rx,ML}}}$ Denoised received signal compensated by $\Delta \hat{f}_{Rx,prior} + \Delta \hat{f}_{Rx,ML}$

$\boldsymbol{argmin}$ Argument of the minimum

$\boldsymbol{Rs}$ Symbol rate

Abbreviations

ACM Adaptive Coding and Modulation. 10, 12

APSK Amplitude and Phase-Shift Keying. 6, 10, 14, 15, 35, 38, 46, 50, 56, 57

AWGN Additive White Gaussian Noise. 6, 22, 23, 27, 34, 38

BER Bit Error Rate. 6, 9, 44, 46, 47, 49, 51, 55

BLUE Best Linear Unbiased Estimator. 27

BPSK Binary Phase Shift Keying. 13, 17, 18, 35

CnC Carrier-in-Carrier. 3, 4, 7, 8, 10, 57

CRLB Cramer-Raw Lower Bound. 24, 25, 28

D&M Delay and Multiply. 23

DA Data-Aided. 16, 17, 23, 27, 28, 35

DD Decision-Directed. 16, 17, 30, 31, 36, 45, 54

DFD Division Free Duplexing. 3

DFT Discrete Fourier Transform. 28, 30

DL Down-Link. 4, 5, 7–9, 37, 56

DoubleTalk® DoubleTalk®. ix, 3–5, 7, 10, 56, 57

DVB Digital Video Broadcasting. xvii, 2, 10, 57

DVB-S Digital Video Broadcasting - satellite. 2

DVB-S2 Digital Video Broadcasting - Satellite - Second Generation. ix, 2, 6, 7, 10, 11, 14, 15, 17, 18, 21–25, 29–31, 35, 36, 40, 41, 46, 51, 56, 57

DVB-S2X Digital Video Broadcasting (DVB)-S2 Extended. 57

DWT Discrete Wavelet Transform. 34

EARC Extraordinary Administrative Radio Conference. 1

ETSI European Telecommunications Standards Institute. 2, 10

FD Full-Duplex. 3, 4, 6–9, 15, 21

FEC Forward-Error-Correction. xvii, 11

FECFRAME Forward-Error-Correction (FEC) Frame. 11, 12, 14

FED Forward Error Detector. 23

FFT Fast Fourier Transform. 28, 30, 35, 42, 43, 45, 47, 48, 52, 54–56

HD Half-Duplex. 3, 8, 15, 35, 36, 40, 49–51, 57

HPF High-Pass Filter. 34

HTS High Throughput Satellite. 3

IBFD In-Band Full-Duplex. 3–6, 56, 57

ICI Inter-Carrier Interference. 6

ITU International Telecommunication Union. 1, 2

L&R Luise and Reggiannini. 24, 25

LDPC Low-Density Parity-Check. 14

LOS Line-Of-Sight. 6, 10

LPF Low-Pass Filter. 34, 46

M&M Mengali and Morelli. 26, 27

ML Maximum-Likelihood. 19, 24, 28, 30, 31, 35, 36, 41–43, 45, 55, 56

MMSE Minimum Mean Square Error. 43, 45

MODCOD Modulation and Coding scheme. 11–13

MSE Mean Square Error. 43, 45

NCO Numerical Controlled Oscillator. 23

NDA Non-Data-Aided. 17

OFDM Orthogonal Frequency-Division Multiplexing. 32

P2P Point-to-Point. 7–9, 56

PCMA Paired Carrier Multiple Access. 3

PER Packet Error Rate. 50

PLFRAME Physical Layer Frame. 11, 46

PLHEADER Physical Layer Header. 11, 13, 14, 17, 35, 43, 45, 46

PLSCODE Physical Layer Signalling Code. 11, 12, 17, 40, 45

PSK Phase Shift Keying. 18, 22, 27, 29

QPSK Quadrature Phase Shift Keying. 14

R&B Rife and Boorstyn. x, 28, 29, 35

RF Radio Frequency. 5, 9, 10, 38

RMSE Root Mean Square Error. ix, x, 6, 23, 24, 29, 47, 48, 51, 52, 55

SATCOM Satellite Communications. 3, 5, 8, 9

SFFD Same-Frequency/single frequency Full-Duplex. 3

SI Self-Interference. 40, 43, 44, 48, 56

SIC Self-Interference Cancellation. 4–6, 9, 10, 32, 38, 41, 42, 52, 53, 56, 57

SIR Signal-to-interference ratio. 40, 52

SNL Space Network List. 2

SNR Signal-to-Noise Ratio. 6, 20, 23, 25–29, 35, 36, 38, 40, 46–52, 55, 57

SOF Start-Of-Frame. 11, 17–19, 39–41, 43, 45

SOI Site Of Interest. 9, 37, 38

SRRC Square Root Raised Cosine. 46

UL Up-Link. 5, 7, 8

VCM Variable Coding and Modulation. 10, 12

VSAT very-small-aperture terminal. 3

WD Wavelet Denoising. 6, 32, 34

XFERFRAME Complex Forward-Error-Correction Frame. 11, 13, 14

ÖZET

BANT-İÇİ TAM-DUPLEKS DVB-S2 TABANLI TABANLI UYDU HABERLEŞME SİSTEMLERİ İÇİN ANAHTAR ALICI-VERİCİ ALGORİTMALARININ YAZILIMSAL UYGULAMALARI

Khaled Walid Elgammal

Elektrik-Elektronik Mühendisliği ve Siber Sistemler, Yüksek Lisans

Tez Danışmanı: Doç. Dr. Mehmet Kemal Özdemir

Ocak, 2021

Günümüzde, Nesnelerin İnterneti (Internet of Things) ve 5G-uydu entegrasyonları gibi uygulamaların hayatımıza girişiyle uydu bant genişliğine olan talep artmaktadır. Bant İçi Tam Çift Yönlü İletişim, uydu rölesinin çift uplink gönderisini tek downlink gönderisine indirgeyerek, uydu-yer bant genişliğini 2 katına çıkartır ve operasyon harcamalarını önemli ölçüde azaltır.

Bu tezde, uydunun bükülmüş bir boru rölesi gibi etki oluşturduğu uydu haberleşme senaryosu için kendiliğinden bozulma senaryosunu geliştiriyoruz ve test ediyoruz. Bu senaryoda, her iki alıcı-vericiden gönderilen iki mesaj uydudaki downlink bant genişliğine ayarlanır. Önerilen sistem, zaman ve frekans sapmaları ve gürültünün bulunduğu durumlarda test edilecektir. Sistem, kendiliğinden bozulmaları ve faz kaymalarını indirgeme yeteneğine sahiptir.

Matlab simülasyonu, önerilen senaryonun, ek sinyal-gürültü oranı maliyetinde, frekans kayması içermeyen geleneksel yarı çift yönlü sisteminkiyle karşılaştırılabilir bir bit hata oranı değeri elde edebileceğini göstermektedir. Ayrıca, iletilen sinyalin yankısında yapılan tahminin ortalama karekök hatası yeterince küçüktür.

Önerilen "dijital video yayını - uydu - ikinci nesil" tabanlı sistem, mobil ana taşıyıcı, IP kanalı, kişisel iletişim ve Denizcilik iletişimi gibi geniş bir uygulama kümesi için kullanılabilir.

Anahtar sözcükler: Tam-Dupleks, Bant-İçi Tam-Dupleks, Aynı-Bant Tam-Dupleks, Paylaşılmış-Frekans Tam-Dubleks, DoubleTalk, CarrierInCarrier, Sat-Com, Taşıyıcı Eşzamanlanması.

ABSTRACT

SOFTWARE IMPLEMENTATION OF KEY TRANSCEIVER ALGORITHMS FOR AN IN-BAND FULL-DUPLEX DVB-S2-BASED SATELLITE COMMUNICATION SYSTEM

Khaled Walid Elgammal

M.S. in Electrical, Electronics Engineering and Cyber Systems

Advisor: Assoc. Prof. Dr. Mehmet Kemal Özdemir

January, 2021

Nowadays, the demand for satellite bandwidth is boosted driven by the introduction of new areas of applications such as 5G-satellite integration and the internet of things. In-Band Full-Duplex communications, where a satellite relay down-converts both uplink messages onto one downlink spectrum carrier, offers doubling the downlink spectrum capacity and reducing the operation expenditure significantly.

In this thesis, we develop and test a self-interference scheme for satellite communication scenario in which the satellite acts as a bent-pipe relay. In this scenario, both messages from both transceivers are set on the same downlink bandwidth at the satellite. The proposed system operates in the presence of time & frequency offsets and noise. The system removes the self-interference and compensates for frequency and residual phase offsets.

Matlab simulation shows that the proposed scheme is able to achieve a bit-error-rate value comparable to that of a frequency-offset-free conventional half-duplex system in the cost of additional signal-to-noise ratio. Moreover, the root-mean-square error in estimating the echo of the transmitted signal is minor.

The proposed "digital video broadcasting - satellite - second generation"-based system can be used for a wide set of applications such as mobile backhaul, IP trunking, personal communications, and Maritime communication.

Chapter 1

Introduction and Motivation

On October 4, 1957, the Soviet Union launched the world's first artificial satellite, Sputnik 1, a polished metal sphere, with four broadcasting radio antennas [10]. Sputnik 1 was used to broadcast radio pulses carrying the information about cosmic rays and pressure [11]. A few months later, on January 31, 1958, the USA launched its first satellite, Explorer 1. It had 2 antennas, which were used to transmit data from multiple scientific instruments to earth [12]. One year later, the International Telecommunication Union (ITU), whose Turkey is a founding member and a contributing country since 1865 [13], held the first Extraordinary Administrative Radio Conference (EARC), in which the first batch of the allocated frequencies for outer space was set available. The gathered delegates in the conference agreed that due to the scarcity and critical importance of frequency spectrum as an asset for radio communications, the frequency allocation should be strictly respected.

Due to the rapid growth in satellite communications, more frequency allocation was needed urgently, thus, by 1963, the number of allocated frequencies had been multiplied 15 times [14]. Since 1963, and for the next 57 years, many ITU events have focused on regulating the spectrum usage of space radio communication services. Today, the ITU constitution holds the main principles that govern the regulation of frequency spectrum allocations to different radio communications

services No. 196 of the ITU Constitution (Article 44) states:

> "In using frequency bands for radio services, Members shall bear in mind that radio frequencies and any associated orbits, including the geostationary-satellite orbit, are limited natural resources and that they must be used rationally, efficiently and economically, in conformity with the provisions of the Radio Regulations, so that countries or groups of countries may have equitable access to those orbits and frequencies, taking into account the special needs of the developing countries and the geographical situation of particular countries"

The article emphasizes the utmost importance of efficient usage of the spectrum, implying the need for developing techniques to achieve it. Thus, the ITU created the Space Network List (SNL), which is a list of basic information concerning satellites and earth stations. SNL Part A informs about the orbits occupancy and the spectrum usage [15]. For the sake of spectrum saving, new techniques need to be developed to increase its compactness and achieve higher capacity.

In September 1993, the DVB project was created with an initial task, to develop a 'pre-standardization' body for different digital broadcasting technologies such as digital cable, terrestrial and satellite broadcasting. One year later, Digital Video Broadcasting - satellite (DVB-S) was ready and in Spring 1995, the first DVB broadcasting services started in Europe. Industrial contributors to the project helped to direct the DVB specifications to serve the market needs. DVB work resulted in European Telecommunications Standards Institute (ETSI) standards for physical layers, error correction, and transport for each delivery medium. DVB-S2 was developed to provide more data capacity with DVB-S backward compatibility. 30% of additional capacity in DVB-S2 was introduced by higher modulation and coding schemes. Currently, all new European digital satellite receivers use DVB-S2 by including the ability to decode DVB-S [16].

Commodities such as gold are naturally rare, and it is because of this rareness that makes it more valuable. Likewise, the spectrum is a rare telecommunication resource. This rarity with high market demand causes a high cost for the channel

bandwidth. In 2003, the cost of very-small-aperture terminal (VSAT) internet for 1 MHz bandwidth per month could vary around 3,500\$ [17]. In 2019, with the introduction of Ka-band High Throughput Satellite (HTS), which mostly has the frequencies $27.5 - 31$ GHz for the uplink and $17.7 - 21.2$ GHz for the downlink, the cost was reduced significantly to few hundred dollars, while it is still high for some other traditional satellites [17].

Satellite Communications (SATCOM) provides connectivity between 2 or more parties on earth. The communication link between those parties can be in one direction from a transmitter to 1 or more receivers, or in 2 directions where every end is transmitting and receiving. In a broadcasting system, e.g., the television channels broadcasting system, only one site is transmitting and the other sites are receiving, which is known as a simplex communication system. The other types of systems where both sites are interchanging messages, e.g., internet users, mobile cellular users, the system is known as a duplex system. A Full-Duplex (FD) system implies simultaneous interchanging of messages, while a Half-Duplex (HD) system implies a non-simultaneous transmission. Most of the FD systems use different spectrum resources to achieve its dual functionality. Meanwhile, In-Band Full-Duplex (IBFD) emerges as a technique to allow FD functionality using the same bandwidth, i.e., without using an additional different spectrum resource.

Multiple names refer to the same technique in the literature, with the most popular of which being IBFD, Same-Frequency/single frequency Full-Duplex (SFFD) [18], and Division Free Duplexing (DFD) [19], [20]. Meanwhile, manufacturers created patented IBFD solutions, such as Paired Carrier Multiple Access (PCMA) by Viasat [21] and DoubleTalk® by Comtech [22], [23].

A variety of SATCOM applications employ simplex [24], HD [25], and FD modes [2]. FD mode is employed by applications such as high speed content delivery, G.703 trunking, disaster recovery, IP trunking, and emergency communications. Thus, deploying an IBFD solution like DoubleTalk® Carrier-in-Carrier (CnC) in these applications gives large operating expenses savings [26], especially for symmetrical links where each user requires the same bandwidth amount and

data rate [27]. Figure 1.1 shows the savings in a CnC link.
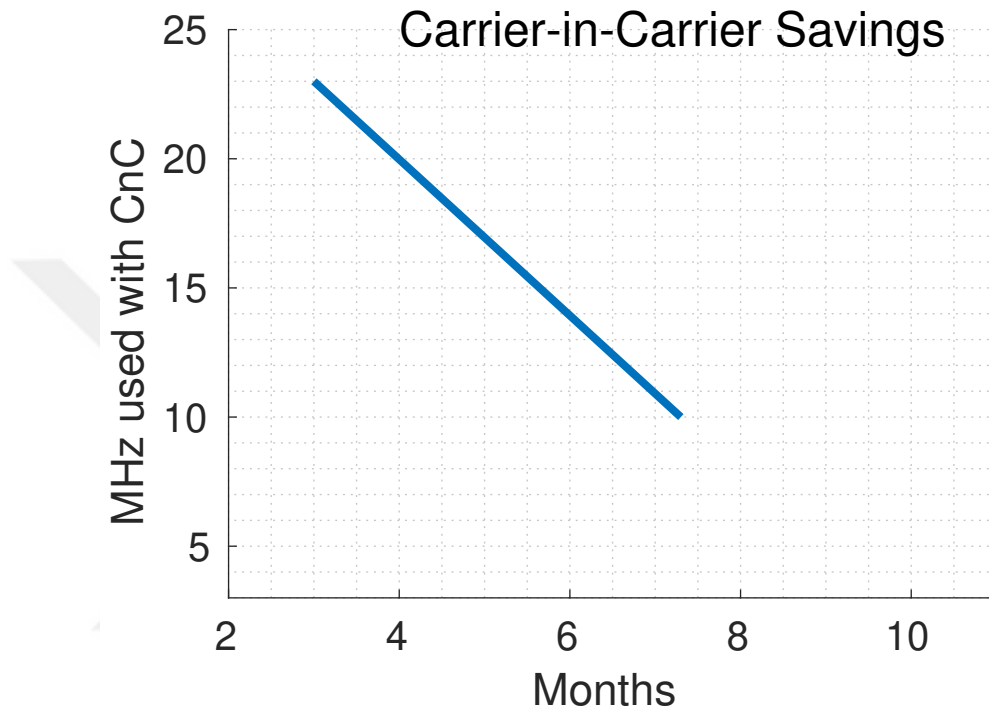
Figure 1.1: Time needed to recover $100k in equipments from savings on satellite bandwidth costs [1]

The key metric to IBFD solutions is their Self-Interference Cancellation (SIC) ability. While SIC requires multiple stages in different domains, DoubleTalk® CnCis a digital SIC systems. A SIC system deployed at one site of a FD satellite link cancels the echo of its transmitted signal, found in the Down-Link (DL). The echo signal undergoes different effects from multiple sources such as the channel effects and non-ideal electronics. However, the SIC technique has to estimate all the changes exercised on the signal upon its arrival in the DL.

Figure 1.2: DoubleTalk® Signal Processing [2]

The idea of IBFD was first proposed and analyzed in [28] in terms of Radio Frequency (RF) SIC. More research followed by more techniques in RF, analog, and digital domains. While most publications relate to the problem in the terrestrial environment, a few discussed it within the SATCOM scope. The authors in [29] studied the feasibility of a satellite relaying system, in which, the Up-Link (UL) to the satellite relay uses the same frequency as the DL from the satellite. [2] examine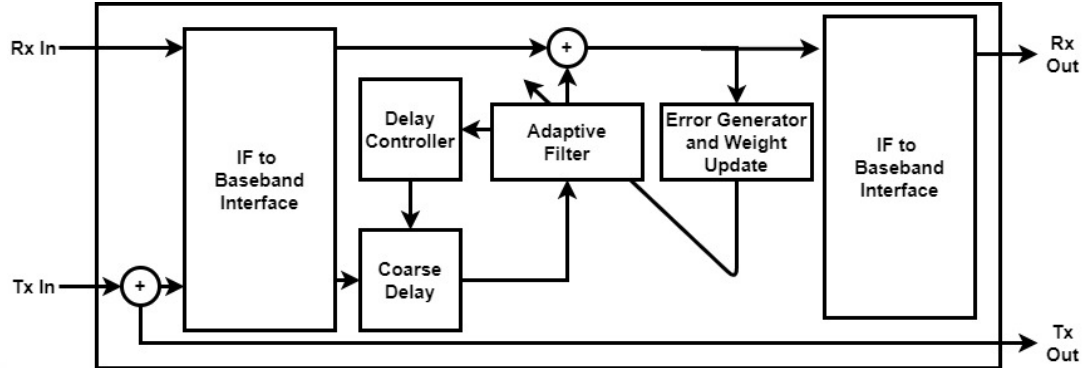d the DoubleTalk® technique and its practical aspects by showing the main issues of the system and its technical approach. [2] also discussed the differences between terrestrial and satellite IBFD problem. In [30], the authors studied a multi-channel transmit/receive module for an S-Band SatCom Phased Array system using signal measurements for rapid testing of the system.

In an IBFD system, the SIC technique should be able to detect and compensate for real-time changes caused by temperature variations, mechanical vibrations, and the motion of things in the environment[2]. Thus, developing a solution like DoubleTalk® has to meet the requirements of the dynamic satellite channel such as:

- The non-static frequency offsets resulting from up and down conversions in addition to frequency translation by the transponder.

- The Doppler shift resulting from the difference in velocity between earth and satellite.

5

- The non-linearities in the processing electronics introducing distortion and Inter-Carrier Interference (ICI).

The channel between the satellite and the earth station is a Line-Of-Sight (LOS) channel and can be considered as a single-path channel. Hence, we assume a single-tap complex-valued channel coefficient for both components of the superimposed signal.

In this thesis, we develop and analyze the performance of an IBFD SIC scheme for pilot-less DVB-S2 systems, employing 16 Amplitude and Phase-Shift Keying (APSK) modulation in a symmetrical link while considering the problems of the frame and frequency synchronization under Additive White Gaussian Noise (AWGN). The overall system performance is measured in terms of desired received signal Bit Error Rate (BER) for different Signal-to-Noise Ratio (SNR) values, while the frequency offset estimation is measured in terms of RMSE.

The rest of the thesis is structured as follows: Chapter 2 reviews the adopted FD scenario and DVB-S2 standard. Chapter 3 gives a short literature review on frame and frequency synchronization techniques for DVB-S2 systems, and Wavelet Denoising (WD). Chapter 4 shows the proposed algorithm and its performance. Finally, the thesis conclusion and possible future work are given in Chapter 5.

Chapter 2

System Model

In this chapter, we will discuss the problem scenario and its solutions given in the literature with a focus on CnC DoubleTalk® system. We will also review the sections of the DVB-S2 standard addressing the physical layer frame structure, the modulation, and the bit mapping. The details in these sections are used to implement our system.

2.1   Scenario

A conventional Point-to-Point (P2P) satellite communication system consists of 2 parties on earth, interchanging messages through a satellite relay. The transmitter on earth transmits its message towards the satellite, the satellite receives the message, and re-transmits it back to the receiver on earth, after changing the carrier frequency. During this processing, additional frequency carrier offsets or shift and time delays are introduced to the messages signals, as well as amplitude and phase modifications.

A FD type system implies that both earth points are transmitting and receiving at the same time using the same spectrum [31]. For most systems today, this is achieved by using different carriers for UL and DL of both ends. These systems

are not operating in a "True" FD mode but rather in a HD mode, because they use different frequencies. FD systems have the ability to transmit and receive at the same time on the same frequency spectrum, i.e., without needing an additional resource.
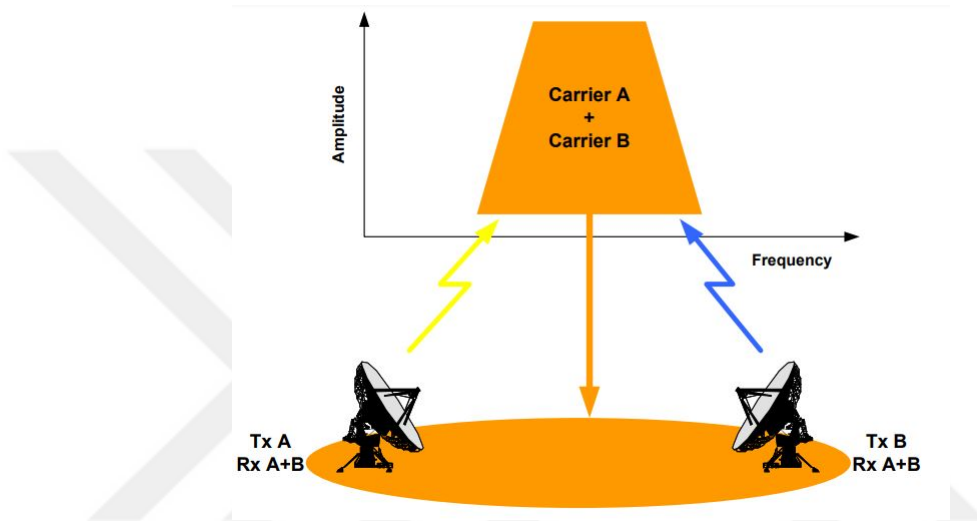
Figure 2.1: FD downlink spectrum [1].

DoubleTalk® CnC offers a FD operation mode in P2P SATCOM [2]. The DL from satellite to both ends is using the same spectrum bandwidth. This is achieved by superimposing the transmitted messages from both ends at the same DL frequency carrier and then sending this superimposed messages from the satellite to both receivers as shown in Figure 2.1[1] Thus, the received superimposed signal has the echo of the transmitted signal and the desired received signal. The example in Figure 2.1 shows the station on the left transmitting message A and the station on the right transmitting message B, while both stations are receiving $A + B$ at the same frequency spectrum. This is different from the FD scenario in which UL and DL use the same spectrum.

Figure 2.2: FD Scenario.

In order to extract the desired received signal, the echo of the transmitted signal has to be removed from the superimposed signal, which is known as SIC. This requires estimating the echo of the transmitted signal with high accuracy. For some time, it was believed that SIC is not possible without 3 different processing phases in RF, analog, and digital domains [2]. Recently, some attempts were made to rely on digital processing solely, as in [32] and [33].

To create an accurate copy of the echo signal, the signal parameters, such as timing offset, amplitude, carrier frequency offset, and phase offset, have to be estimated and tracked. Low accuracy in estimating these parameters would cause significant degradation in the BER of the received signal [34]. Figure 2.2 shows a FD P2P SATCOM scenario in which the Site Of Interest (SOI) transmits the message S_T and aims to receive the message S_R from another site. In the DL superimposed signal arriving at the SOI, the echo of S_T is affected by time delay Δd_T, frequency offset Δf_T, phase offset $\Delta \phi_T$ and channel coefficient α_T, while S_R is affected by time delay Δd_R, frequency offset Δf_R, phase offset $\Delta \phi_R$ and channel coefficient α_R. Thus, the self-interference canceller should be able to estimate Δd_T, Δf_T, $\Delta \phi_T$ and α_T with high accuracy.

9

In this work, the satellite-earth channel is assumed to be a flat fading LOS channel and hence, only a single path is considered. Each of the 2 components of the superimposed signal is affected by a complex-value channel coefficient.

DoubleTalk® CnC requires that the satellite must be a non-processing satellite, which performs only amplification, filtering, and frequency conversions. This satellite is referred to as a "bent pipe" satellite, in which no baseband modulation/demodulation is applied. Instead, only RF processing is employed. In this satellite model, the transmitted signal is looped back to earth in the same beam.

2.2   DVB-S2 Standard

DVB-S2 standard is widely used in different satellite applications including those incorporating DoubleTalk® systems. Hence, the proposed SIC algorithm complies with the standard and exploits it. The DVB-S2 standard was introduced in 2003 by ETSI as a successor to DVB-S standard to permit more flexibility and capacity efficiency using newly introduced modulation and coding techniques. APSK high order modulation schemes such as 16-APSK were included in the new version. Additionally, DVB-S2 allowed unique length, modulation, and coding schemes for every frame using Adaptive Coding and Modulation (ACM) and Variable Coding and Modulation (VCM) modes. In this section, we develop a basic understanding of the standard and its frame structure.
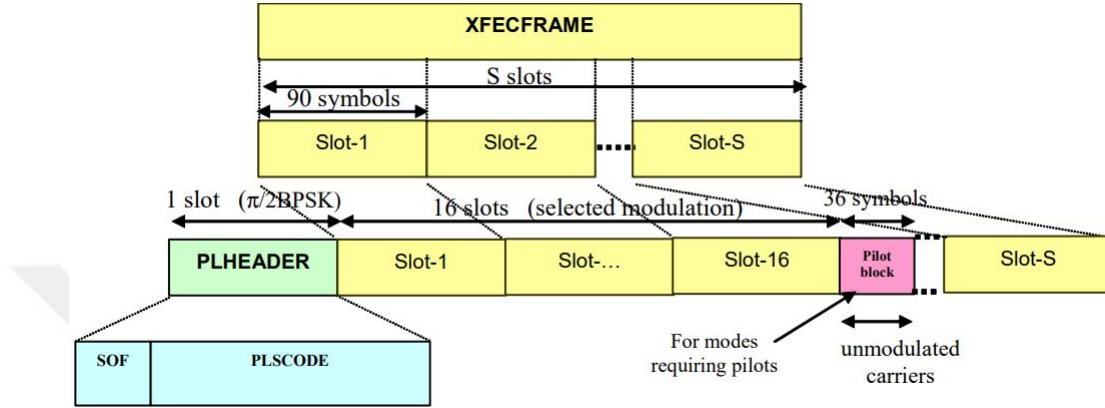
2.2.1 DVB-S2 Framing structure

Figure 2.3: PLFRAME architecture [3].

Figure 2.3[3] shows the detailed description of DVB-S2 Physical Layer Frame (PL-FRAME). A PLFRAME consists of a Physical Layer Header (PLHEADER) and a Complex Forward-Error-Correction Frame (XFERFRAME). The PLHEADER is used for receiver synchronization and physical layer signaling. The receiver synchronization implies signal parameters estimation and tracking in order to restore the signal's shape before transmission. These parameters include the amplitude, time delay, frequency offset, and phase offset. Physical layer signaling intends to inform the receiver about the form of signal that is used to represent the data bits. [3] The XFERFRAME contains the encoded frame payload divided into slots of 90 symbols each. Optional 36-symbols pilots may be inserted for every 16 slots. Pilots help to facilitate carrier frequency and phase synchronization at the cost of 2.4% of the frame capacity.

The PLHEADER starts with a 26-symbols preamble called Start-Of-Frame (SOF) that corresponds to the hexadecimal sequence $18D2E82$. The remaining 64 symbols of the PLHEADER hold the encoded Physical Layer Signalling Code (PLSCODE) bits. A PLSCODE contains the encoded information about the XFERFRAME modulation, FEC rate, FEC Frame (FECFRAME) length and the presence/absence of pilots. XFERFRAME modulation and FEC rate are specified by the 5 bits of Modulation and Coding scheme (MODCOD) field, while

11

FECFRAME length and state of pilots are specified by the 2 bits of TYPE field. Both MODCOD and TYPE are encoded by the linear block code G to generate the PLSCODE, as shown in Fig 2.4, where

$$G = \begin{bmatrix} 0101010101010101010101010101010101 \\ 0011001100110011001100110011 \\ 0000111100001111000011110000111 \\ 0000000011111111000000001111111 \\ 0000000000000000111111111111111 \\ 1111111111111111111111111111111 \end{bmatrix}. \quad (2.1)$$

Finally, the PLSCODE is scrambled by the sequence:
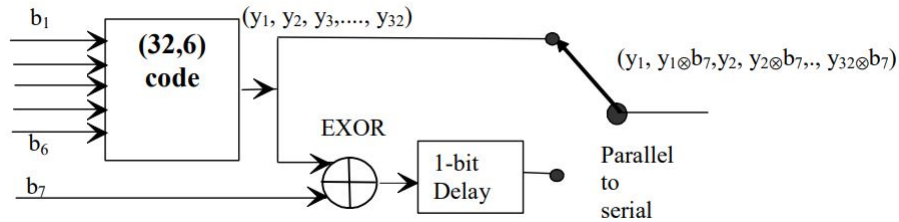0111000110011101100000111100100101010011010000100010110111111010

Figure 2.4: PLSCODE generation[3].

Modulation and coding schemes can vary on a frame-by-frame basis in DVB-S2 under VCM or ACM. When applied, VCM can provide error protection levels based on service components. If a return channel is available, it can be used with ACM functionality to provide further protection and adaptation to channel characteristics.

2.2.2 DVB-S2 Modulation

The PLHEADER bits are modulated into 90 $\pi/2$ Binary Phase Shift Keying (BPSK) symbols according to the rule [3]:

$$I_{2i-1} = Q_{2i-1} = (1/\sqrt{2})(1 - 2y_{2i-1}),$$
$$I_{2i} = -Q_{2i} = -(1/\sqrt{2})(1 - 2y_{2i}) \qquad (2.2)$$
$$for\, i = 1, 2, ..., 45$$

Additionally, if existing, the pilot should be 36 un-modulated symbols, identified by $I = (1/\sqrt{2}), Q = (1/\sqrt{2})$. The XFERFRAME modulation and code rate follow the MODCOD 5-bits field, according to Table 2.1[3].

Mode	MODCOD	Mode	MODCOD
QPSK 1/4	1_D	8PSK 9/10	17_D
QPSK 1/3	2_D	16APSK 2/3	18_D
QPSK 2/5	3_D	16APSK 3/4	19_D
QPSK 1/2	4_D	16APSK 4/5	20_D
QPSK 3/5	5_D	16APSK 5/6	21_D
QPSK 2/3	6_D	16APSK 8/9	22_D
QPSK 3/4	7_D	16APSK 9/10	23_D
QPSK 4/5	8_D	32APSK 3/4	24_D
QPSK 5/6	9_D	32APSK 4/5	25_D
QPSK 8/9	10_D	32APSK 5/6	26_D
QPSK 9/10	11_D	32APSK 8/9	27_D
8PSK 3/5	12_D	32APSK 9/10	28_D
8PSK 2/3	13_D	Reserved	29_D
8PSK 3/4	14_D	Reserved	30_D
8PSK 5/6	15_D	Reserved	31_D
8PSK 8/9	16_D	DUMMY PLFRAME	0_D

Table 2.1: Modulation and coding corresponding MODCOD [3].

DVB-S2 works in continuous stream fashion, in contrast to burst mode standards. This means that the transmission lasts, even if there is no data to transmit. Thus, if no XFERFRAME is ready for transmission, a Dummy PLFRAME is sent. A Dummy PLFRAME consists of a PLHEADER and 36 slots of unmodulated complex symbols with real and imaginary components $I = Q = 1/\sqrt{2}$. The continuous transmission feature allows the receiver to use the current received frame to identify the beginning of the following frames, as long as the symbol timing synchronization is preserved and the current frame length is known [35].
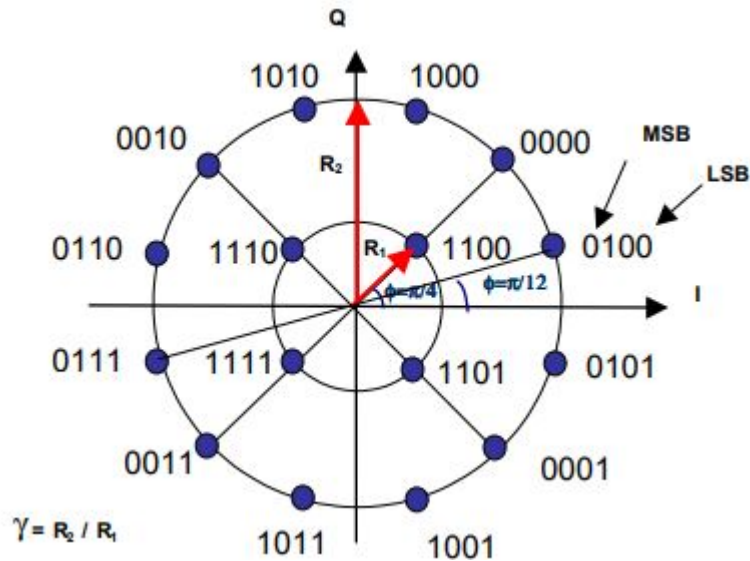
2.2.3 Bit Mapping

Figure 2.5: Bit mapping for 16APSK in DVB-S2 [3].

In DVB-S2, FECFRAME bits are mapped into Gray coded absolute APSK, for Quadrature Phase Shift Keying (QPSK) and 8APSK. For 16APSK, 2 concentric rings points are used as shown in Figure 2.5, where η is the constellation radius ratio, which is varied based on the code rate according to the values in [3]. The constellations of high order modulation schemes are optimized to allow the operation over non-linear transponders. Additionally, the combination of 16/32APSK with Low-Density Parity-Check (LDPC) codes can achieve the proper system

14

operation over non-linear satellite channel. 16APSK allows high spectrum efficiency in interactive applications, especially in multi-beam satellites employing pre-distortion schemes[36]. FD systems offer doubling this spectrum efficiency existing in traditional HD DVB-S2 systems[27].

2.3   Conclusion

This chapter explained the FD scenario for which this thesis is dedicated. It showed the parameters to be estimated to reach a valid solution. Additionally, the chapter presented the exploited details of the employed standard, and highlighted the compliance with DVB-S2 standard and its physical framing structure.

Chapter 3

A Review of Synchronization Techniques and Introduction to Wavelet Denoising

A communication system receiver's first task is to restore a received signal's shape to its original shape upon reception. To achieve this task, the receiver has to synchronize the received signal by compensating for various channel's effects, such as fading, time delay and Doppler frequency offset in addition to the carrier frequency offset and phase offset resulting from non-ideal electronics.

After downconversion and sampling of the received signal, the aforementioned effects can be canceled in the digital domain. Processing in the digital domain gives high flexibility and ease of implementation. All the methods and techniques in this thesis are in the digital domain. The methods of synchronization for the aforementioned effects can be classified into 3 categories:

- Data-Aided (DA) methods: where the receiver uses known symbol sequence(s) as reference

- Decision-Directed (DD) methods: where the receiver uses detected symbols values as reference

- Non-Data-Aided (NDA) methods: where the receiver doesn't use known or detected symbols.

While the DA techniques have the best synchronization performance at the cost of transmission capacity in the form of training sequences and pilots, the DD methods can cause error propagation in symbols [37]. However, the NDA techniques don't consume extra transmission bandwidth and can provide accurate parameter estimation at the cost of processing complexity [38]. To achieve acceptable performance without using extra bandwidth, hybrid techniques are developed [38].

In a DVB-S2 receiver, the synchronization of the received signal parameters is performed in order. Following the symbols timing recovery and sampling, comes the frame synchronization, then the frequency and phase offset compensation. Each synchronization step might require several steps to be achieved, e.g. the frequency synchronization step consists of coarse and fine synchronization steps. The following sections review some of the most popular DVB-S2 frame and frequency synchronization techniques for conventional receivers.

3.1 Frame Synchronization Techniques for DVB-S2 Systems

The DVB-S2 transmission consists of frames, with a preamble at the beginning of each frame. In order to extract a frame's payload, an essential step is to decode the PLSCODE. The PLSCODE holds the information about the frame length, frame modulation and coding, and additional information required for message extraction. Due to that, PLSCODE detection is essential for the functionality of the receiver.

To successfully decode PLSCODE, a frame synchronization step, prior to all other steps, is required. In this step, SOF and PLSCODE are used for finding the frame edges. The PLHEADER, where both fields exist, is modulated by $\pi/2$-BPSK modulation, which rotates the signal constellation 90° for every symbol.

The $\pi/2$-BPSK modulation reduces the signal fluctuations in comparison with the classic BPSK scheme [39]. Frame synchronization techniques search for the preamble in the received signal using cross-correlation operations. The correlation output value hits a threshold when the correlated sequences relatively match. The following subsections discuss a few of the correlation schemes used in DVB-S2.

3.1.1 Conventional Cross-Correlation

In this algorithm, the received symbols $r(k)$ are correlated with the complex reference SOF field symbols $c(k)$, where $k = 0, 1, ...L-1$ and L is the SOF length. Assuming the received signal has symbol rate $1/T_s$, and experiences frequency offset Δf_o and phase offset Θ_o , the noiseless k-th symbol of the received signal's preamble is

$$r(k) = c(k)e^{j(2\pi k \Delta f_o T_s + \Theta_o)} \tag{3.1}$$

The SOF correlation with the received preamble is

$$R(m) = \left| \sum_{k=0}^{L-1} r(k+m)c^*(k) \right| \tag{3.2}$$

where $(.)^*$ is the complex conjugate and m is the correlation index and the symbols offset between the correlated sequences. If the received preamble is exactly correlated at the beginning of the SOF, then the noiseless correlation is

$$R(0) = \left| \sum_{k=0}^{L} r(k)c^*(k) \right| = \left| \sum_{k=0}^{L} |c(k)|^2 e^{j(2\pi k \Delta f_o T_s + \Theta_o)} \right| \tag{3.3}$$

As it can be seen from Eq. (3.3), the frequency offset affects the correlation value, which may lead to serious degradation in correlation performance, unless additional measures are taken.

3.1.2 Choi-Lee Detector

In [40], Choi and Lee proposed a frame synchronization technique for Phase Shift Keying (PSK) systems that is robust to frequency and phase offsets. Their

technique was derived from Maximum-Likelihood (ML) criterion and L_0 to L_3 estimators. A short overview of the equations to calculate L_0 to L_3 estimators is given here, but further details about performance can be found in [40]. The estimators are as follows:

$$L_0(m) = \sum_{i=1}^{L-1} \left\{ \left| \sum_{k=i}^{L-1} r^*(m+k)c(k)r(m+k-i)c^*(k-i) \right|^2 - \sum_{k=m+i}^{m+L-1} |r(k)|^2 \, |r(k-i)|^2 \right\}$$
(3.4)

$$L_1(m) = \sum_{i=1}^{L-1} \left\{ \left| \sum_{k=i}^{L-1} r^*(m+k)c(k)r(m+k-i)c^*(k-i) \right| - \sum_{k=m+i}^{m+L-1} |r(k)| \, |r(k-i)| \right\}$$
(3.5)

$$L_2(m) = \left| \sum_{k=1}^{L-1} r^*(m+k)c(k)r(m+k-1)c^*(k-1) \right| - \sum_{k=m+1}^{m+L-1} |r(k)| \, |r(k-1)|$$
(3.6)

$$L_3(m) = \left| \sum_{k=1}^{L-1} r(m+k)c^*(k)r^*(m+k-1)c(k-1) \right|$$
(3.7)

where m is the position, $m \in [0, N-1]$ and N is the number of symbols in a frame.

3.1.3 Differential Correlation

Proposed by Choie and Lee in [40], L_3 introduces a differential detector that calculates the correlation, named as $R_{diff}(m)$, on a pairwise differential basis. That is,

$$R_{diff}(m) = \left| \sum_{k=0}^{L-2} r(k+m) \cdot r^*(k+m+1) \cdot (c(k) \cdot c^*(k+1))^* \right| = \left| \sum_{k=0}^{L-2} R(k+m) \right|$$
(3.8)

If the SOF is exactly positioned at the beginning of received signal's preamble, i.e. $m = 0$, and using the noiseless received signal's preamble model in Eq. (3.1)

$r(k) = c(k)e^{j(2\pi k \Delta f_o T_s + \Theta_o)}$, then

$$r(k+1) = c(k+1)e^{j(2\pi (k+1)\Delta f_o T_s + \Theta_o)} \tag{3.9}$$

$$
\begin{aligned}
r(k).r^*(k+1) &= c(k)e^{j(2\pi k \Delta f_o T_s + \Theta_o)}.c^*(k+1)e^{-j(2\pi (k+1)\Delta f_o T_s + \Theta_o)} \\
&= c(k).c^*(k+1).e^{-j(2\pi \Delta f_o T_s)}
\end{aligned} \tag{3.10}
$$

Correlating the differentials with preamble differentials and substituting by Eq. (3.1) gives:

$$
\begin{aligned}
R_{\text{diff}}(0) &= \left| \sum_{k=0}^{L-2} r(k) \cdot r^*(k+1) \cdot (c(k) \cdot c^*(k+1))^* \right| \\
&= \left| \sum_{k=0}^{L-2} c(k) \cdot c^*(k+1) \cdot e^{-j2\pi \Delta f_o T_s} \cdot c^*(k) \cdot c(k+1) \right| \\
&= \left| \sum_{k=0}^{L-2} |c(k)|^2 \cdot |c(k+1)|^2 \, e^{-j2\pi \Delta f_o T_s} \right| \\
&= \underbrace{\left| e^{-j2\pi \Delta f_o T_s} \right|}_{1} \left| \sum_{k=0}^{L-2} |c(k)|^2 \cdot |c(k+1)|^2 \right|
\end{aligned} \tag{3.11}
$$

From Eq. (3.11) we can see that differential correlation is independent of the phase and frequency offset.

The optimal differential frame detector in [4] can achieve frame synchronization using 4 frames under large frequency offset of 5 MHz at sampling rate of $25 MSymbols/s$ and low SNR of -2.3 dB. Its acquisition probability under different frequency offset is shown in Figure 3.1[4].
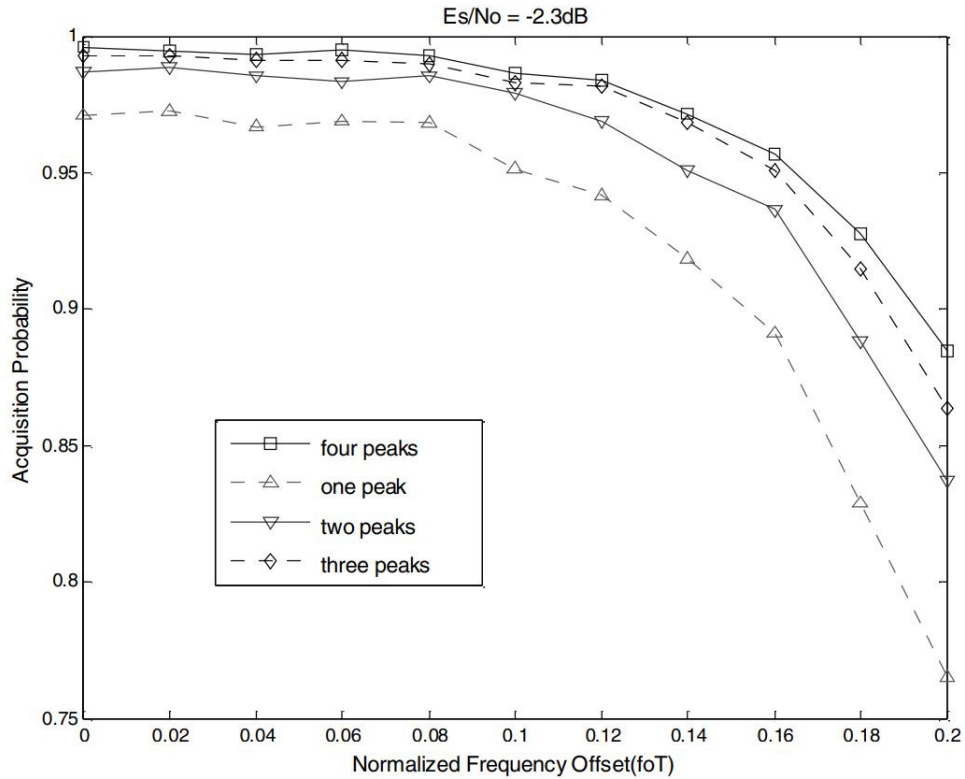
Figure 3.1: Acquisition probability for different searching peaks [4].

3.2 Frequency Synchronization Techniques for DVB-S2

Estimating the frequency offset for both the transmitted signal and the received signal is of critical importance in FD systems. Usually, frequency synchronization is performed in 2 steps, i.e., Coarse and fine frequency synchronization. The coarse step compensates for initial large frequency offset, while the fine step tracks small variations in carrier frequency. A conventional DVB-S2 receiver finds the preamble and training pilots to apply coarse frequency synchronization followed by fine frequency tuning.

The frequency mismatch in the received signal is due to different effects besides the Doppler shift. Naturally, the frequency oscillators in the transmitter and receiver don't have an identical oscillating frequency. Hence, any frequency oscillator is characterized by a frequency tolerance value, which indicates the amount of possible deviation from nominal oscillating frequency.

Additionally, the changing environmental conditions contribute effectively to the frequency mismatch [41]. In quartz oscillators, these environmental conditions include: the temperature and its rate of change, magnetic fields, variations in the rates of hitting ionizing electromagnetic radiations, and the consistent growth of radiation due to its accumulation [42]. In a satellite environment, a solar flare can cause a deterministic change in the oscillating frequency while humidity can cause both deterministic and stochastic variations [43]. Other Instabilities include aging, noise, frequency change with acceleration and power supply voltage. Aging causes long term frequency drift [44], while short-term instabilities almost always result from noise[45]. Acceleration effects, such as earth gravitation, change the oscillating frequency of atomic and quartz oscillators [46].

Assuming the received signal sample, having a sampling rate $1/T_s$, after the ideal matched filter and ideal time sample at $k.T_s$ is $r(k)$:

$$r(k) = c(k)e^{j(2\pi\Delta f_o kT_s + \Theta_o)} + n(k) \tag{3.12}$$

where $c(k)$, Δf_o and Θ_o are the M-ary PSK complex-valued transmitted symbol, the frequency offset and the phase offset, respectively. $n(k)$ is complex AWGN sample, with zero mean and unit variance. If the first L symbols of $c(k)$ are the known preamble by the receiver, then a beat signal $z(k)$ resulting from mixing $r(k)$ with $c(k)$ can be obtained as follows:

$$z(k) = r(k)c^*(k) = e^{j(2\pi\Delta f_o kT_s + \Theta_o)} + n^{'}(k), \quad 0 \leq k \leq N - 1 \tag{3.13}$$

where $n^{'}$ is an AWGN term resulting from $n(k)c^*(k)$ with zero mean and unit variance. In this section, we review the most common techniques of frequency synchronization in DVB-S2.

3.2.1 Closed Loop Frequency Error Detector / Delay and Multiply
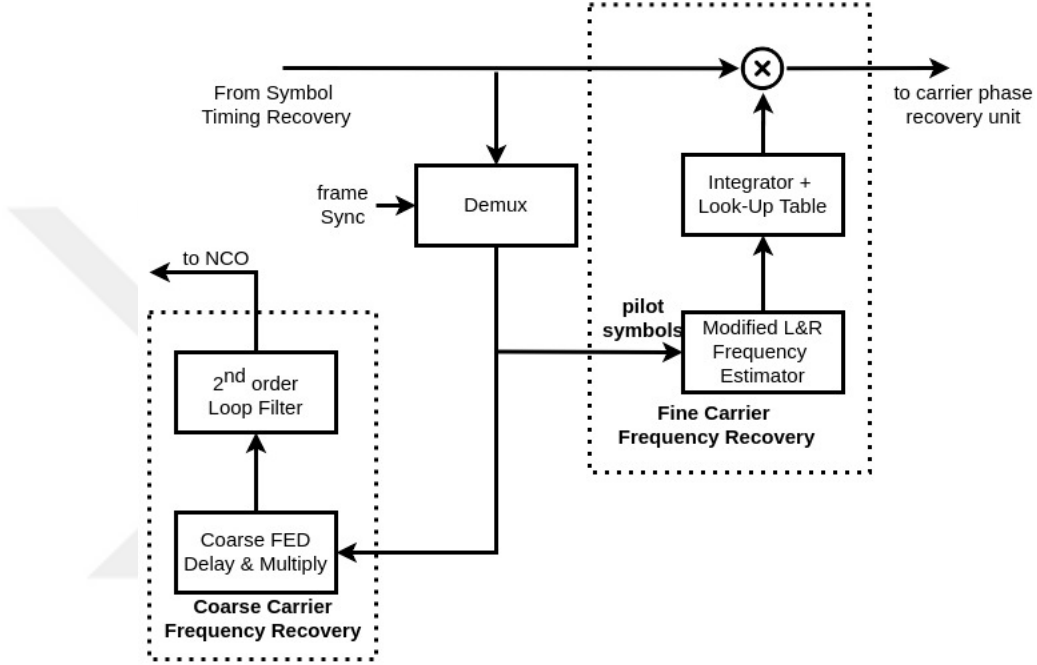

Figure 3.2: FED D&M DVB-S2 digital demodulator [5].

A DA pilot-based Forward Error Detector (FED) known as Delay and Multiply (D&M) method that is dedicated for coarse frequency synchronization. Its detectable frequency offset can reach as high as 20% of the symbol rate. It is integrated with a feedback loop as shown in Figure 3.2. D&M is functional only on pilot fields, and requires finding $e(k)$ as given in the following equation:

$$e(k) = Im\{z(k)z^*(k-2)\} \tag{3.14}$$

$e(k)$ represents the error value that the FED finds by applying D&M, which is then filtered and fed to a Numerical Controlled Oscillator (NCO) to compensate for the frequency offset. Figure 3.3 shows the RMSE of the detected frequency offset, for DVB-S2 coarse frequency estimation in AWGN channel, normalized to the symbol rate at different SNRs. The FED loop has a normalized bandwidth of 10^{-4}. According to [5], the required synchronization time to reach this performance is

100 ms at 25 MSymbols/s, using data-free successive pilot fields. Therefore, at this feeding rate, 1650 pilot fields are required.
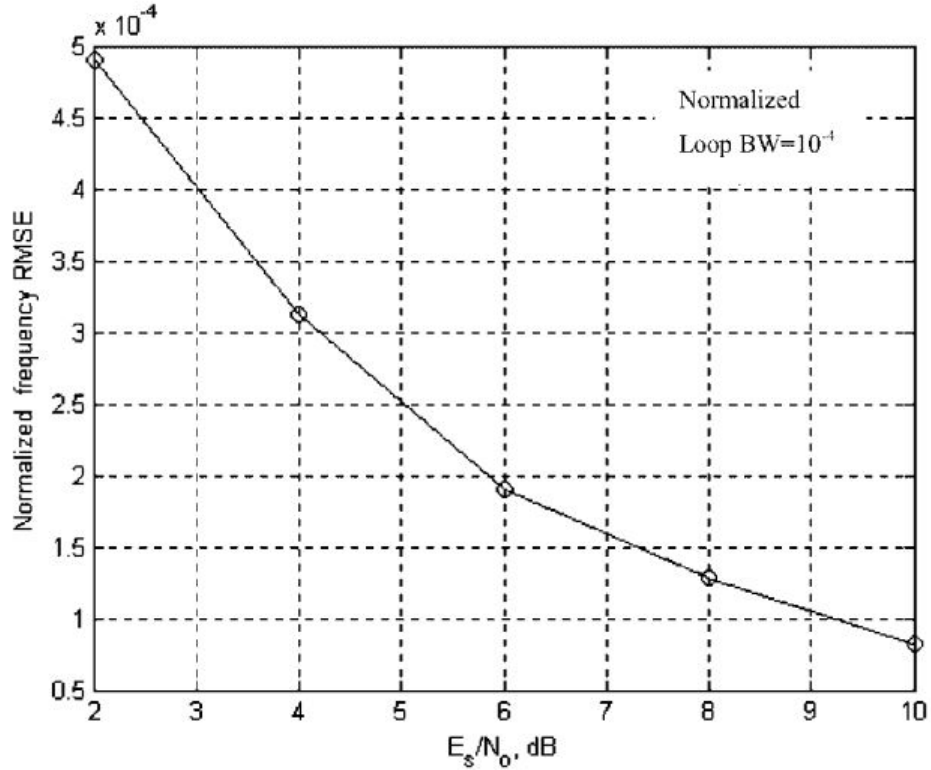

Figure 3.3: Normalized frequency RMSE of FED coarse frequency estimation in DVB-S2 [5].

3.2.2   Luise and Reggiannini's Method

Luise and Reggiannini (L&R) is a ML approach to find the frequency offset in received samples. It provides the estimates close to the Cramer-Raw Lower Bound (CRLB) with moderate computational complexity. The estimated frequency offset $\Delta \hat{f}$ is given by

$$\Delta \hat{f} = \frac{1}{\pi(M+1)} \arg \left\{ \sum_{k=1}^{M} R(k) \right\} \tag{3.15}$$

where M, the auto-correlation length, is a design parameter, and $R(k)$ is the estimated correlation evaluated as

$$R(k) = \frac{1}{N-k} \sum_{m=k}^{N-1} z(m) z^*(m-k) \tag{3.16}$$

where N is the signal length. The optimum value for M is $N/2$, at which CRLB is achieved even for low SNR [47]. Despite that, the value of M limits the absolute detectable frequency offset by $1/(M+1)$.

3.2.3 Averaged Luise and Reggiannini Frequency Synchronization Method

In [5], the method of L&R is used for DVB-S2 fine frequency tracking due to its low complexity and high accuracy, even at low SNR. However, a coarse frequency synchronization step must be applied before L&R to mitigate large offsets. The authors in [5] proposed averaging the auto-correlation over multiple consecutive pilots to achieve even higher accuracy. The detected frequency offset becomes:

$$\Delta \hat{f} = \frac{1}{\pi(M+1)} \angle \sum_{l=1}^{L} \sum_{m=1}^{M} R_l(m) \tag{3.17}$$

where $R_l(m)$ is the l-th pilot auto-correlation calculated over $M = N/2$ lags. Figure 3.4 shows the performance of averaged L&R estimator compared to CRLB at different SNRs. It can be seen that the averaged L&R almost reaches CRLB even at very low SNR.
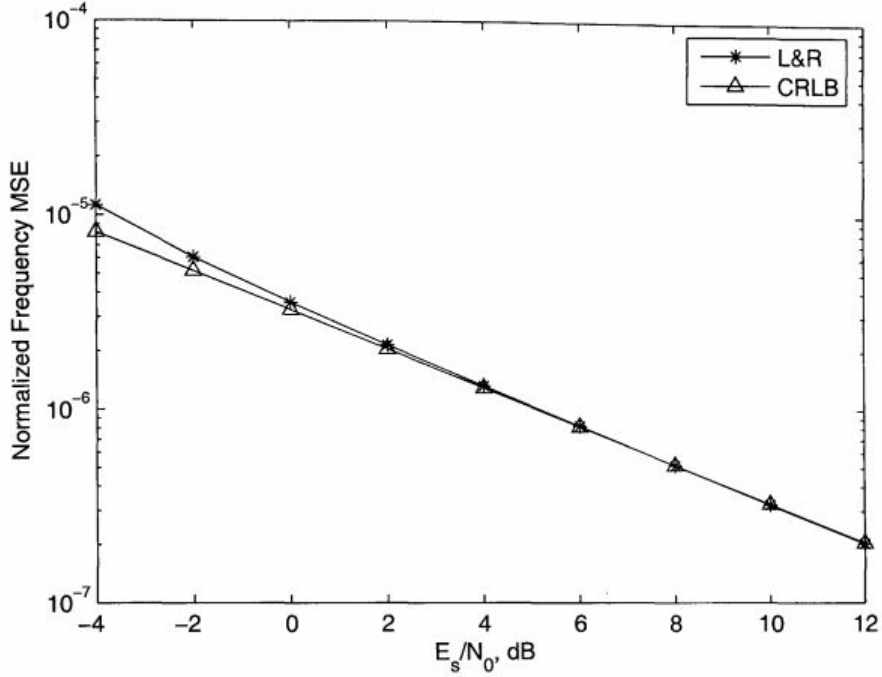
Figure 3.4: Frequency MSE for L&R's estimator; $N = 36$ and $\Delta f_o = 0.01$ [6].

3.2.4 Mengali and Morelli's Method

In [48], Mengali and Morelli (M&M) estimated the frequency offset with high accuracy, even at low SNR, using auto-correlation $R(m)$ as follows

$$R_{M\&M}(m) = \frac{1}{N-m} \sum_{k=m}^{N-1} z(k)z^*(k-m), \quad 1 \le m \le M \qquad (3.18)$$

where M is a design parameter value not greater than $N/2$. Substituting Eq. (3.12) into $R(m)$, the auto-correlation becomes as follows:

$$R_{M\&M}(m) = e^{j2\pi m \Delta f_o T_s}[1 + \zeta(m)] \qquad (3.19)$$

with

$$\zeta(m) = \frac{1}{N-m} \sum_{k=m}^{N-1} [\tilde{n}(k) + \tilde{n}^*(k-m) + \tilde{n}(k)\tilde{n}^*(k-m)] \qquad (3.20)$$

Assuming that the SNR $>> 1$, then $R_{M\&M}(m)$ can be rewritten as:

$$R_{M\&M}(m) \approx B_m e^{j(2\pi m \Delta f_o T_s + \zeta_I(m))} \qquad (3.21)$$

where B_m is the amplitude and $\zeta_I(m)$ is the imaginary component of $\zeta(m)$. As we have

$$\angle R_{M\&M}(m)R_{M\&M}^*(m-1) = 2\pi\Delta f_o T_s + \zeta_I(m) + \zeta_I(m-1) \qquad (3.22)$$

Then, the frequency offset can be found by applying determined weights $w_(m)$ as follows:

$$2\pi\Delta\hat{f} = \sum_{m=1}^{M} w(m)\angle R_{M\&M}(m)R_{M\&M}^*(m-1); \quad 1 < m \leq M \qquad (3.23)$$

where optimal M value is $N/2$, and $w(m)$ is found by a Best Linear Unbiased Estimator (BLUE) through the function in [48] as

$$w(m) = \frac{3[(N-m)(N-m+1) - M(N-M)]}{M(4M^2 - 6MN + 3N^2 - 1)}; \quad 1 < m \leq M \qquad (3.24)$$

M&M is DA suitable for PSK modulation and can achieve optimal accuracy for a frequency offset range of $\pm 20\%$ of the sampling rate.

3.2.5 Fitz Method

In [49], Fitz proposed a DA technique based on the auto-correlation of $z(k)$:

$$R(m) = \frac{1}{L_p - m} \sum_{k=m}^{L_p-1} z(k)z^*(k-m), \quad 1 \leq m \leq N - 1 \qquad (3.25)$$

where L_p is the pilot symbol length. By substituting Eq. (3.13) in $R(m)$, we get:

$$R(m) = e^{j2\pi\Delta f_o m T_s} + n''(m), \quad 1 \leq m \leq N - 1 \qquad (3.26)$$

where n'' is AWGN with zero mean and unit variance. Assuming that the SNR is sufficiently high, so that $n'' << 1$, then the error $e(m)$ should be relatively small, where

$$e(m) = \arg R(m) - 2\pi\Delta f_o m \qquad (3.27)$$

given that

$$P < \frac{1}{2|\Delta f_{o,max}|T_s}, \quad P \leq N/2 \qquad (3.28)$$

27

where here, P is a design parameter and $\pm\Delta f_{o,max}$ is the uncertainty range of Δf_o. Averaging the error over P yields

$$\frac{1}{P}\sum_{m=1}^{P}e(m) = \frac{1}{P}\sum_{m=1}^{P}\arg R(m) - \pi(P+1)\Delta f_o T_s \qquad (3.29)$$

The left-hand side can be considered as zero as its terms tend to compensate each other, thus solving the right-hand side gives:

$$\Delta\hat{f} = \frac{1}{\pi P(P+1)T_s}\sum_{m=1}^{P}\arg\{R(m)\} \qquad (3.30)$$

Fitz estimator is unbiased for $|\Delta f_o| \leq 1/(2PT_s)$ and reaches CRLB for $P = N/2$. As number of samples P increases, estimation accuracy increases, the estimated frequency range gets wider and the computational complexity increases.

3.2.6 Rife and Boorstyn's Method

In [7], R&B proposed a DA ML algorithm, that uses the Discrete Fourier Transform (DFT) to estimate a single tone parameter from discrete time signal as shown in Eq. (3.31). DFT can be implemented using Fast Fourier Transform (FFT) algorithm. R&B's algorithm consists of 2 search steps: coarse and fine. The coarse frequency estimation gives an approximate value of the frequency offset and limits the search for the DFT peak, while the fine search determines the exact value. DFT size M in coarse search should be power of 2 and have the size $2N$ or $4N$, where N is the signal length. The FFT is as follows:

$$Z(f) = \frac{1}{N}\sum_{k=0}^{N-1}z(k)e^{-j2\pi kfT_s} \qquad (3.31)$$

R&B estimator has the normalized frequency range from -0.5 to 0.5 and can achieve very high accuracy even at low SNR, with a limited number of samples, as shown in Figure 3.5. Additionally, R&B estimator has a low frequency offset sensitivity, which implies that the variation of the frequency offset has a minimal impact on accuracy.
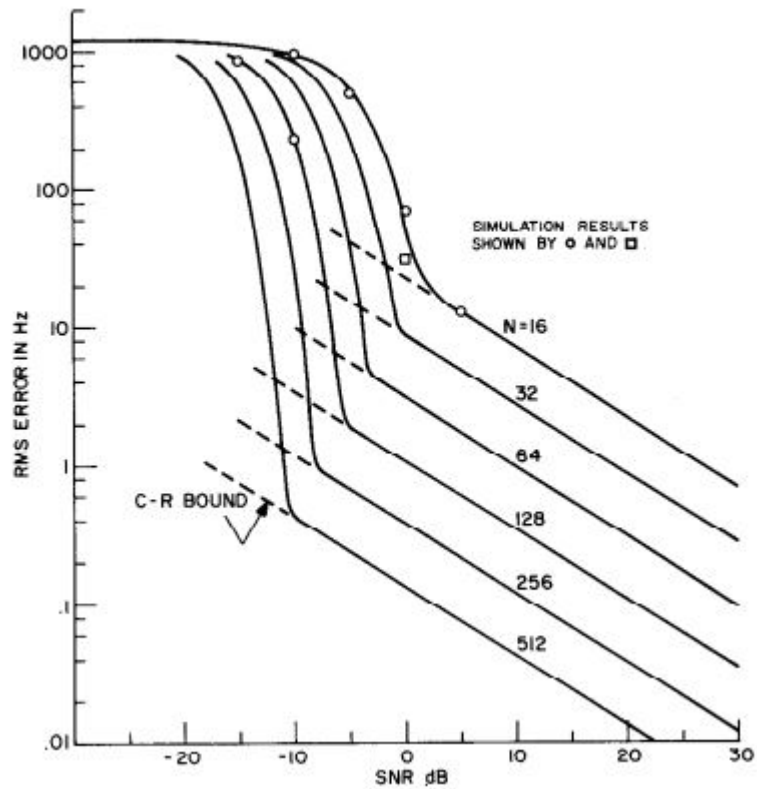
Figure 3.5: Frequency RMSE of R&B estimator for a 2KHz signal at sampling frequency of 4Khz [7].

In this section, we reviewed some of the most popular frequency synchronization techniques that can be used with M-ary PSK modulation such as in DVB-S2 standard. While multiple techniques have high accuracy, R&B's method preserves that accuracy even at very low SNR.

3.3   Phase Synchronization Techniques for DVB-S2

Usually, a small frequency offset remains after the frequency synchronization. For that, a phase synchronization step follows the frequency synchronization. In

this section, we review the most common phase offset estimation techniques for DVB-S2 receivers.

3.3.1 Feed-Forward Maximum-Likelihood Phase Estimation

The feed-forward ML phase estimator uses $z(k)$ to estimate the phase offset in the received signal as shown in Eq. (3.32) [6]:

$$\hat{\Theta}_o = \angle \sum_{k=0}^{L-1} z(k) \tag{3.32}$$

where $\hat{\Theta}_o$ is the estimated phase offset. The feed-forward ML estimator is proved to be efficient in [50].

3.3.2 Discrete Fourier Transform Maximum-Likelihood Phase Estimation

The DFT ML phase estimation follows the FFT ML frequency estimation step. After we find the FFT using Eq. (3.31), we select the frequency at which the $Z(f)$ is maximum as shown in Eq. (3.33):

$$\Delta \hat{f}_{ML} = \arg \max_f |Z(f)| \tag{3.33}$$

where $\Delta \hat{f}_{ML}$ is the FFT ML estimated frequency offset. Then, we can find the phase offset as follows:

$$\hat{\Theta}_0 = \angle \{\exp(-j2\pi \Delta \hat{f}_{ML} k T_s) Z(\Delta \hat{f}_{ML})\} \tag{3.34}$$

3.3.3 Decision-Directed Phase Estimation

The DD phase synchronization is a feedback technique that uses detector's symbol decision. The phase error $e(k)$ is detected and compensated recursively on a
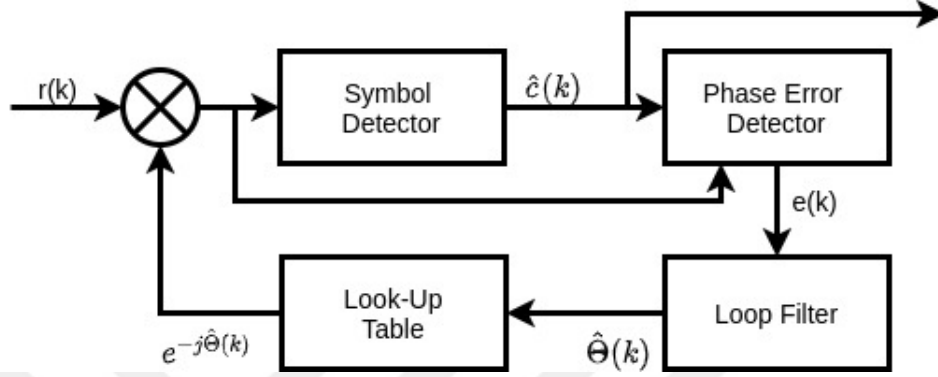
symbol-by-symbol basis as shown in Figure 3.6.

Figure 3.6: Decision-directed phase synchronization

The loop filter filters the phase error to minimize the fluctuations and provide an estimated phase error $\hat{\Theta}(k)$. The look-up table creates the compensating signal using the detected phase offset of the current symbol as shown in Eq. (3.35)

$$\hat{\Theta}(k+1) = \hat{\Theta}(k) + \gamma e(k) \tag{3.35}$$

where γ is step size parameter.

In this section, we reviewed the most common phase synchronization techniques that can be employed in DVB-S2 systems. ML techniques have good performance in case that the phase can be tracked over the frame, using the pilots. Meanwhile, the DD technique can work in a pilot-independent fashion.

3.4 Wavelet Denoising

A wavelet is a mathematical function that decomposes a given input function into different scale components. Every scale component can be assigned a frequency range and has a resolution that matches its scale. In Fourier analysis, a given time signal is transformed to its frequency equivalent, with the loss of time information. While a wavelet transform preserves the time information by variable sized windows. A long time interval is employed where low-frequency information

exists and a short time interval is employed where high-frequency exists. On the other hand, Fourier analysis uses sinusoids as the basis functions, while wavelet analysis has more complicated basis functions that vary in time and frequency like the wavelets shown in Figure 3.7 [51].

The wavelet analysis was firstly proposed by Alfred Haar in 1909. Since that time, it was used in many fields including telecommunications, e.g. wavelet Orthogonal Frequency-Division Multiplexing (OFDM). Despite the long history of wavelet analysis, wavelets were barely used in SIC applications. Recently, [52] used the wavelet decomposition to denoise a self-interfering channel. To the best of the author's knowledge, this is the first time WD is used in SIC. In this thesis, the wavelet is used for denoising the desired received signal after removing the self-interference component as will be shown in the following chapter.

WD works by thresholding the signal after transforming it using the wavelet transform. The wavelet transforms the signal into a sparse representation, where small value coefficients represent the noise. Removing these coefficients denoises the signal efficiently. Although conventional filtering is usually used for removing out-of-band high-frequency noise, it fails to remove the noise overlapping with the signal spectrum. This is due to the fact that the functionality of a typical filter is based on its Fourier spectra. Meanwhile, the wavelet promotes the difference in amplitudes of the signal and noise, rather than the location of their frequency components. Thus, a shrinkage in the amplitude can be translated to noise reduction, regardless of the frequency component's location, which allows removing the in-band noise [53].
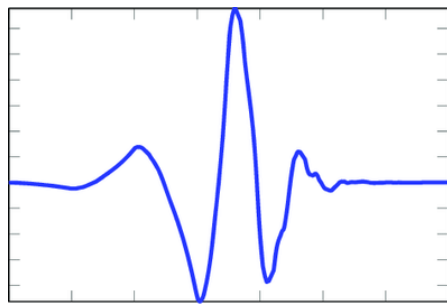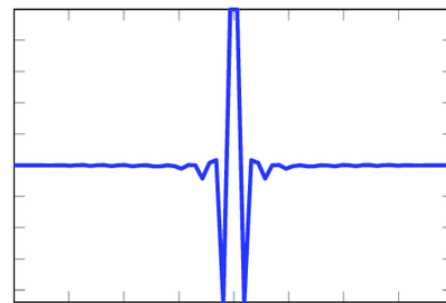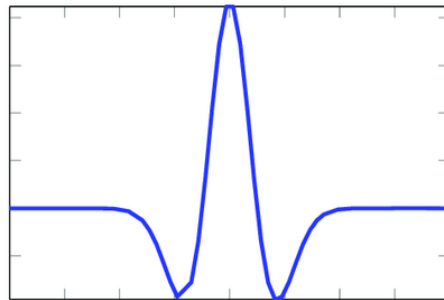
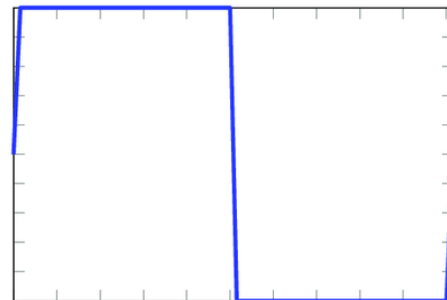(a) db Wavelet
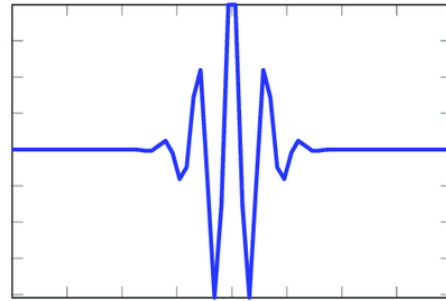
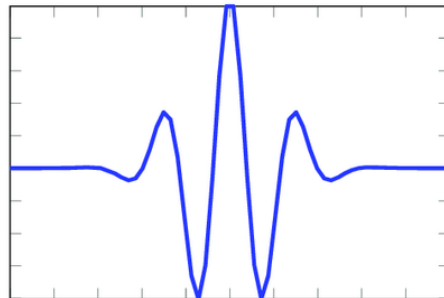(b) Morlet Wavelet
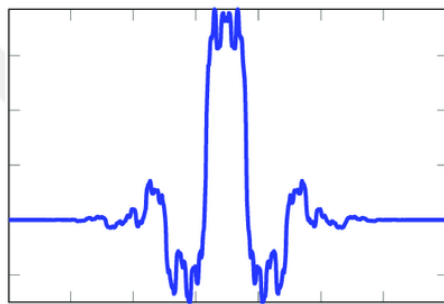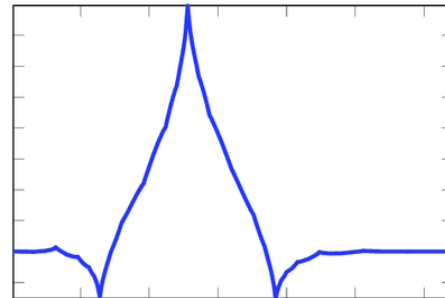
(c) Biorthogonal Wavelet

(d) Spline Wavelet

(e) Mexican Hat Wavelet

(f) Haar Wavelet

(g) Gaussian Wavelet

(h) Coiflet Wavelet

Figure 3.7: Examples of Wavelet basis functions [8].

To understand how WD works, we assume the observed received signal r consists of the desired signal c and AWGN n:

$$r[k] = c[k] + \sigma a[k], \quad 0 \leq k \leq N - 1 \tag{3.36}$$

where σ is the noise standard deviation and N is the received signal length. The observed signal in wavelet transformation domain is

$$R_{sym} = C + \sigma A \tag{3.37}$$

where $R_{sym} = \boldsymbol{W}r$, $\boldsymbol{W}$ is the transformation matrix. For $\hat{C}$, the estimator of C, and $\hat{c}$, the estimator of c, we define a diagonal linear projection as

$$\hat{C} = \boldsymbol{\Delta} R_{sym} \tag{3.38}$$

where $\boldsymbol{\Delta} = diag(\delta_0, \delta_1, ... \delta_{N-1}), \delta_i \in [0, 1]$. We find $\hat{c}$ by

$$\hat{c} = \boldsymbol{W}^{-1}\hat{C} = \boldsymbol{W}^{-1}\boldsymbol{\Delta} R_{sym} = \boldsymbol{W}^{-1}\boldsymbol{\Delta}\boldsymbol{W}r \tag{3.39}$$

While $\boldsymbol{W}$ represents the wavelet decomposition into a sparse domain, $\boldsymbol{\Delta}$ is the thresholding matrix, which removes the noise and $\boldsymbol{W}^{-1}$ is the inverse wavelet transform, returning the noiseless signal into its original domain.

The wavelet decomposition process comprises filtering the signal using a High-Pass Filter (HPF) and a Low-Pass Filter (LPF) as shown in Figure 3.8. The filtered signals are decimated by a factor of 2. The decimated output values of the HPF are the coefficients of level 1 of Discrete Wavelet Transform (DWT). The output values of the LPF are then re-filtered and decimated again using the same filters to give the next level DWT coefficients. In every level, the time resolution is reduced by the half, while the frequency resolution of the LPF output is doubled. In this way, the time localization of frequency components is preserved, although its resolution depends on its level. High-frequency components have precise time localization, while low-frequency components have enough time localization.
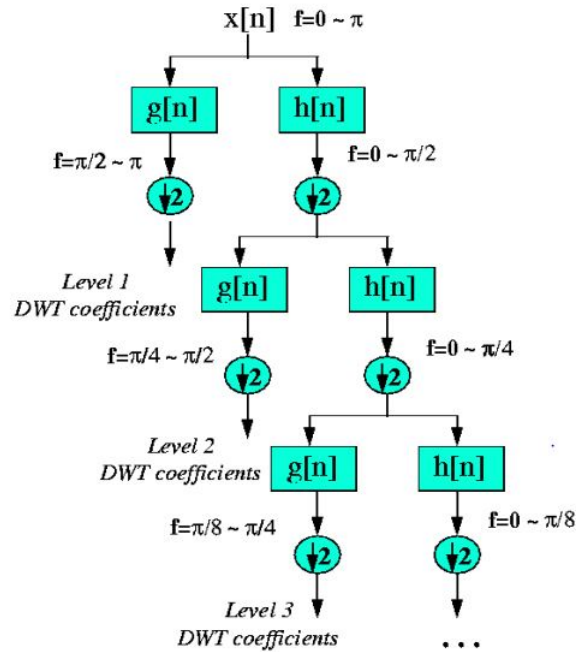
Figure 3.8: Wavelet decomposition process[9]

3.5 Conclusion

In this chapter, we discussed the most popular approaches of frame, frequency ,and phase synchronization for DVB-S2 standard, i.e. 16APSK modulated signals. Additionally, we briefly touched on the wavelet transform and its functionality in denoising the noisy signals.

We discussed multiple correlation-based frame synchronization schemes. In general, frame synchronization methods in DVB-S2 systems tend to exploit the unique BPSK modulation of the PLHEADER section of the frames. The ML differential correlation technique proved to have the best performance for HD conventional DVB-S2 receivers under large frequency offset and low SNR.

Additionally, we discussed 6 of the most popular frequency synchronization techniques for DVB-S2 systems.The DA ML FFT-based technique known as R&B

proved to give high accuracy for large frequency offset range under low SNR in HD conventional DVB-S2 receivers.

Moreover, we briefly reviewed 3 phase synchronization methods. While the ML methods give good performance, they need pilot fields to track the phase change over the frame. On the other hand, DD phase synchronization doesn't need pilots.

Finally, we discussed the wavelet denoising approach and how it can be used to cancel the in-band interference. In the following chapter, we will describe the proposed algorithm and we will evaluate its performance.

Chapter 4

Proposed Algorithm and Results

In this chapter, we will first show the superimposed signal model, its components, and the challenges to be resolved. Then, we will describe the proposed algorithm in detail. Lastly, we will discuss the simulation results under different conditions.

4.1 Signal Model

The proposed system is valid for the scenario in which 2 ground stations are interchanging messages at the same time, by using the same DL spectrum from a satellite to both sites, SOI and the other site, as shown in Figure 2.2. This system shall be employed at both receivers and aims to suppress the echo of transmitted messages and extract the received signals after compensating for frequency offset.
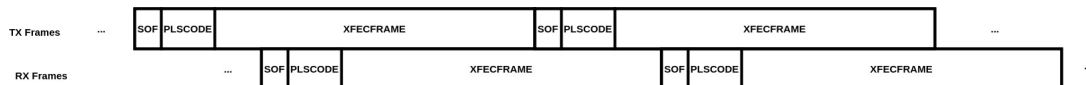

Figure 4.1: Superimposed signal structure.

The scenario in Sec. 2.1 implies that the received baseband superimposed signal S consists of the arriving transmitted signal echo STx_{echo} and the arriving desired

received signal S_{Rx} as shown in Eq. (4.1).

$$S[k] = STx_{echo}[k] + S_{Rx}[k] + n[k] \tag{4.1}$$

where n is AWGN with zero mean and variance σ_n^2. The k-th samples of both STx_{echo} and S_{Rx} suffer from frequency offset as follows:

$$STx_{echo}[k] = \alpha_T Tx[k].e^{j2\pi\Delta f_{Tx}.k.Ts} \tag{4.2}$$

$$S_{Rx}[k] = \alpha_R Rx[k].e^{j2\pi\Delta f_{Rx}.k.Ts} \tag{4.3}$$

where Tx, Rx, Δf_{Tx} and Δf_{Rx} are the original transmitted signal, the original desired received signal, the frequency offsets of the transmitted signal, and the frequency offset of the received signal, respectively. α_T and α_R are the channel coefficients for the transmitted signal and received signal, respectively. As described in Sec. 2.2, both Tx and Rx are APSK modulated. We use 16-APSK modulation for both signals in our system. The 16APSK and 32APSK modes are mainly targeted to contribution applications and can also be used for broadcasting, but this requires a higher level of SNR and the use of advanced predistortion methods in the uplink station to minimize the effect of transponder non-linearity[54]. Additionally, 16APSK scheme provides high spectral efficiency with a SNR requirement that is not as high as the SNR required for 32APSK modulation scheme[3].

No assumptions are made regarding the RF or the analog parts of the receivers as the proposed system falls in the category of a digital SIC. In this system, we assume perfect timing recovery for received samples. Thus, the problem of time synchronization is not discussed.

4.2   Algorithm description

For the SOI, the structure of S is shown in Figure 4.1, where every received frame interferes with a transmitted frame. The system functionality begins by

acquiring the samples of S and consists of the following 2 major steps as shown in Figure 4.2:

1. STx_{echo} estimation and mitigation

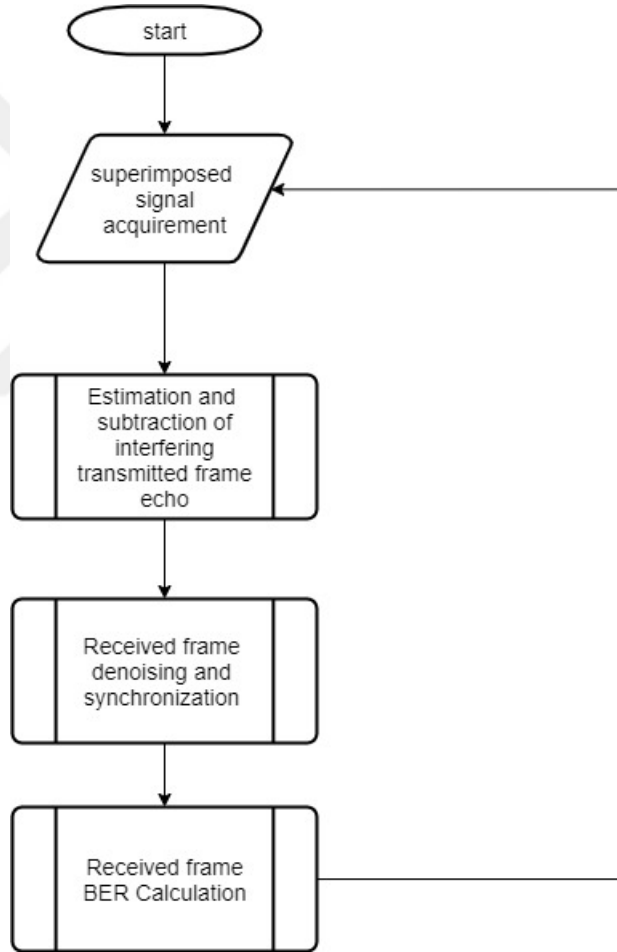2. S_{Rx} denoising and synchronization

Figure 4.2: The proposed overall system processing.

Prior to the 2 middle steps, the system finds the edges of STx_{echo} and S_{Rx} in S. This is achieved by correlating the known SOF signal samples with received S samples in the buffer, as shown in Eq. (4.4), and searching for the correlation peaks. While advanced synchronization schemes, such as in [4] and [39], provide

high performance in conventional HD receivers even at low SNR, they were found to perform poorly in our problem due to high interference between transmitted and received symbols. In our problem, the Signal-to-interference ratio (SIR) is 0 dB which means that the Self-Interference (SI) signal has the same power as the desired received signal. Furthermore, DVB-S2 is characterized by providing a constant stream. Thus, acquiring a single frame is sufficient to track the following frames.

Constant stream indicates that the frames are transmitted continuously, even if there is no information to transmit. In case of no information, a dummy frame is transmitted as explained in Sec. 2.2. Once a frame is found, it is easy to track the following frames by finding the size of the current frame from its PLSCODE [35]. The correlation $R(m)$ is found by

$$R(m) = \sum_{k=0}^{L} S(k+m)c^*(k) \tag{4.4}$$

where L is the preamble length and $c(k)$ is the k-th SOF sample.

SOFs are found in buffer at the correlation peaks, with ambiguity about the peak correspondence to STx_{echo} or S_{Rx}. To find out which peak is coming from SI, another correlation operation with the Tx is required. Here, the discriminator of peaks is another correlation operation with the part of Tx that follows the SOF field. The part used in the discrimination operation includes several slots, in addition to PLSCODE. When S is correlated with the discriminator part of Tx, the highest peak will correspond to Tx, revealing the location of STx_{echo} in S. The mth discrimination correlation value R_{Tx} is found by:

$$R_{Tx}(m) = \sum_{k=L+1}^{L_{Tx}} S(k+m)c^*(k) \tag{4.5}$$

where L is the length of the DVB-S2 preamble and the correlation length is $L_{Tx} - L$.

S_{Rx} is processed after fully removing SI, i.e. for Figure 4.1, both transmitted frames are removed before any processing onto the first shown received frame.

Acquiring the beginning of the transmitted frame's echo leads to find the following transmitted frame by exploiting the constant transmission feature and confirms the location of the desired received frame. As the frame length of the transmitted frame is known, the echo of the following transmitted frame is expected to be received after the end of the current frame, while the desired received frame is expected to have its SOF before that.

4.2.1　Transmitted Frame Cancellation

Figure 4.3 shows the proposed SIC algorithm for DVB-S2. $\Delta \hat{f}_{Tx}$, $\Delta \hat{f}_{Tx,prior}$, $\Delta \hat{f}_{Tx,ML}$ and $\hat{Tx}_{echo}$ are the estimated frequency offset of the transmitted frame, the estimated frequency offset of the prior transmitted frame, the ML estimated frequency offset of the transmitted frame and the estimated echo of the transmitted signal, respectively.
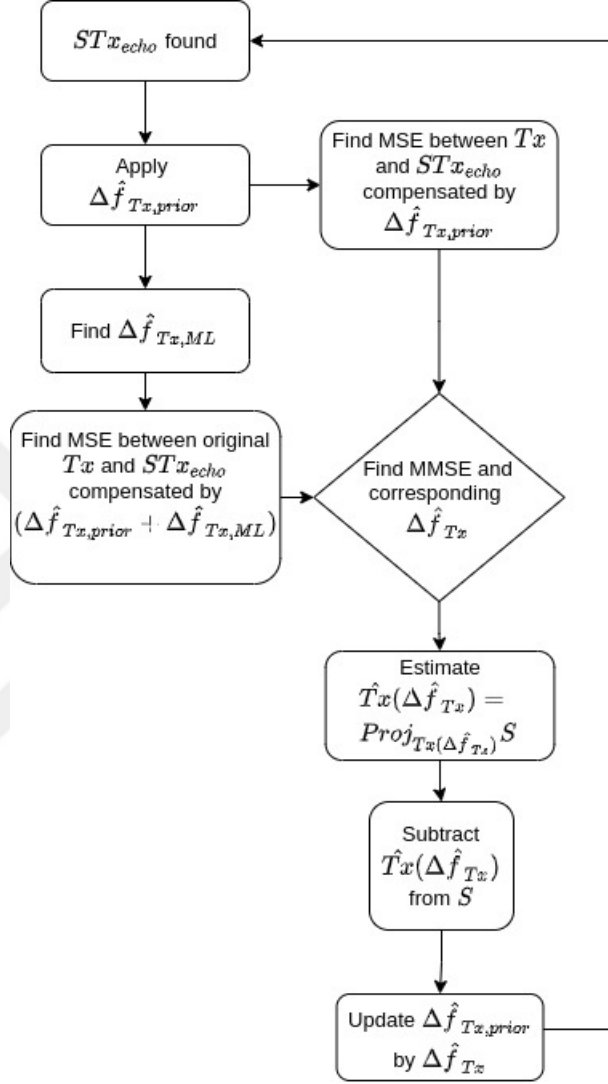
Figure 4.3: SIC algorithm.

The algorithm starts when the edges of STx_{echo} are found. STx_{echo} is compensated for its frequency offset by the value of the estimated frequency offset of the prior transmitted frame $\Delta \hat{f}_{Tx,prior}$. Another frequency offset estimation step is applied to track the change in carrier frequency offset on a frame by frame basis, $\Delta \hat{f}_{Tx,ML}$, using ML FFT method.

SIC requires high accuracy in estimating STx_{echo}, which imposes a constraint on the accuracy of frequency offset estimation. Meanwhile, FFT suffers from the limited resolution that inversely depends on its size. In order to increase

42

the resolution, large FFT is required, which is considered as a burden in terms of complexity. Due to FFT limited resolution, an additional Minimum Mean Square Error (MMSE) frequency estimation is applied. The Mean Square Error (MSE) between the originally transmitted signal Tx and its echo in superimposed signal STx_{echo} compensated by the $\Delta\hat{f}_{Tx,prior}$ is found. Also, the MSE between Tx and STx_{echo} compensated by $\Delta\hat{f}_{Tx,prior} + \Delta\hat{f}_{Tx,ML}$ is found. Then, the MMSE is found and the corresponding frequency offset is considered as the estimated frequency offset $\Delta\hat{f}_{Tx}$.

The ML FFT frequency estimation for the echo of the transmitted signal occurs in 3 steps. The first 2 steps use the SOF and PLHEADER for coarse and fine frequency estimation, respectively. A third step is applied using the whole frame, including the payload, to estimate any residual frequency offset with high accuracy [55]. The length of the employed FFT operations should be long enough to provide accurate estimation.

The following step is to estimate the transmitted signal echo $\hat{T}x(\Delta\hat{f}_{Tx})$ and subtract it from the superimposed signal. For that, we project the superimposed signal S onto the originally transmitted signal shifted by the estimated frequency offset $Tx(\Delta\hat{f}_{Tx})$ as shown in Eq. (4.6)

$$\hat{T}x(\Delta\hat{f}_{Tx}) = Proj_{Tx(\Delta\hat{f}_{Tx})}S \qquad (4.6)$$

This step finds the magnitude of the transmitted signal component in the superimposed signal, which guarantees that the signal that will be removed has the SI as a single basis. That basis depends on the estimated echo of the transmitted signal only and independent of other components such as the desired received signal and noise. In this way, we reduce the risk of damaging the desired received signal.

At this point, $\hat{T}x(\Delta\hat{f}_{Tx})$ is expected to be almost identical to the echo of the transmitted signal in S, thus a simple subtraction operation follows to remove the SI. The final step is to update $\Delta\hat{f}_{Tx,prior}$ by the value of $\Delta\hat{f}_{Tx}$.

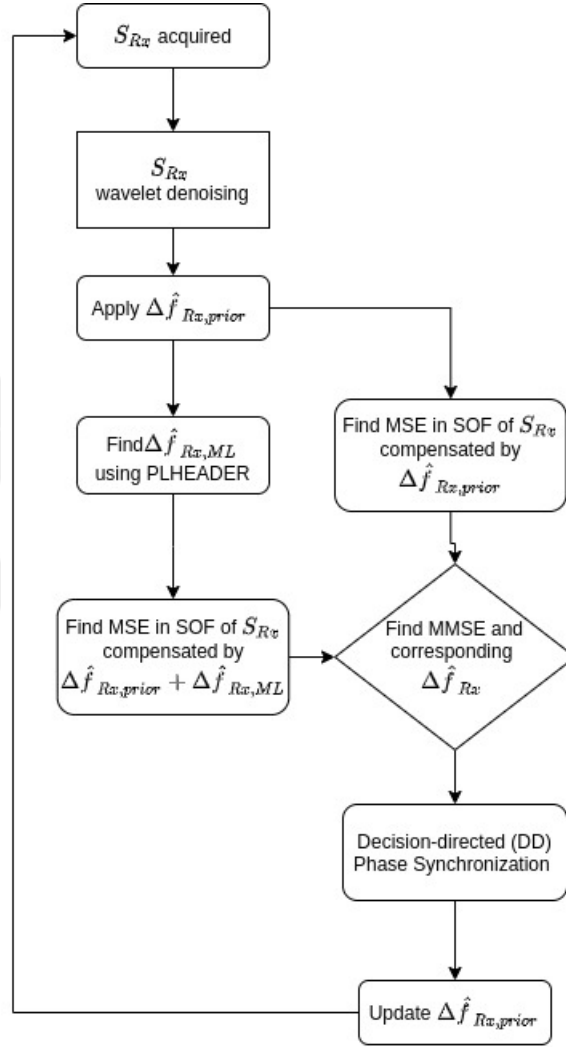## 4.2.2 Received signal denoising and synchronization

Figure 4.4: Frequency synchronization algorithm for desired received frame.

After estimating and removing the echo of the transmitted signal, the received signal is processed to remove the residue of the SI, if any, the noise and to compensate for frequency and phase offsets. The diagram in Figure 4.4 shows the processing steps of the desired received signal. The desired received signal part of the superimposed signal S_{Rx} is denoised using a level 4 symlet wavelet decomposition. The type and level of decomposition are empirically found to achieve the best BER performance. Unlike the work in [52], in our work, we denoise the

desired received signal instead of the SI channel.

The denoised signal is then compensated for prior frequency offset $\Delta \hat{f}_{Rx,prior}$ estimated from previously received frame as shown in Eq. (4.7).

$$S_{Rx,d,\Delta \hat{f}_{Rx,Prior}}(k) = S_{Rx,d}(k).e^{-j2\pi\Delta \hat{f}_{Rx,prior}kT_s} \tag{4.7}$$

where $S_{Rx,d}(k)$ and $S_{Rx,d,\Delta \hat{f}_{Rx,Prior}}(k)$ are the kth symbols of the denoised received signal and the denoised received signal compensated by prior frequency offset $\Delta \hat{f}_{Rx,Prior}$, respectively. Then, the MSE of reference SOF signal and S_{Rx} compensated by $\Delta \hat{f}_{Rx,prior}$ is found as shown in Eq. (4.8).

$$MSE(c, S_{Rx,d,\Delta \hat{f}_{Rx,Prior}}) = \frac{1}{L}\sum_{k=0}^{L-1}\left|c(k) - S_{Rx,d,\Delta \hat{f}_{Rx,Prior}}(k)\right|^2 \tag{4.8}$$

This synchronization step might be sufficient in case of a small frequency shift. Otherwise, if the frequency shift is high enough to be detected by the ML FFT frequency estimator, then the ML estimated frequency offset in received frame $\Delta \hat{f}_{Rx,ML}$ is found in a 2-step frequency synchronization process as explained in [56]. In this process, the coarse frequency offset is estimated using the SOF. Compensating for the coarse offset allows to decode the PLSCODE for the fine frequency synchronization using all the 90 symbols of the PLHEADER.

The MSE of reference SOF signal and S_{Rx} compensated by $\Delta \hat{f}_{Rx,prior} + \Delta \hat{f}_{Rx,ML}$ is found as shown in Eq. (4.9) and compared to the MSE found earlier.

$$MSE(c, S_{Rx,d,\Delta \hat{f}_{Rx,Prior}+\Delta \hat{f}_{Rx,ML}}) = \frac{1}{L}\sum_{k=0}^{L-1}\left|c(k) - S_{Rx,d,\Delta \hat{f}_{Rx,Prior}+\Delta \hat{f}_{Rx,ML}}(k)\right|^2, \tag{4.9}$$

where is $S_{Rx,d,\Delta \hat{f}_{Rx,Prior}+\Delta \hat{f}_{Rx,ML}}(k)$ is the kth symbols of $S_{Rx,d}$ compensated by $\Delta \hat{f}_{Rx,Prior} + \Delta \hat{f}_{Rx,ML}$. The frequency offset achieving the MMSE is selected as shown in Eq. (4.10) and its corresponding signal is finally synchronized using a DD scheme, that works on a symbol-by-symbol basis.

$$\Delta \hat{f}_{Rx} = argmin_{\Delta \hat{f}}MSE \tag{4.10}$$

Due to non-ideal frequency synchronization, a phase offset is continuously changing in the recovered symbols. Due to that, the DD phase synchronization

step is required. In this step, the remaining phase offset is compensated. The phase shift is detected and tracked over symbols. A LPF is used to smooth the detected phase values to remove the phase fluctuations. The closest constellation point is then found and chosen as the recovered symbol.

4.3 Simulation Setup and Results

In this section, the simulation parameters are stated and the system performance is analyzed. The system is developed to support 16-APSK modulation, with the received and transmitted frames experiencing different frequency shift values and under low SNR. We measure the overall system performance in BER, that is, the system output bits that are different from the actual received bits. Extensive Matlab simulations show that the system has the ability to reach the same BER as the un-coded DVB-S2 16-APSK modulation, at the cost of a small increase in SNR.

4.3.1 Complexity Analysis

4.3.2 Simulation Parameters

In this simulation, we use signals generated by superimposing the random symbols of 2 trains of DVB-S2 PLFRAMEs. Each PLFRAME consists of upsampled 32400 16-APSK modulated symbols, in addition to a PLHEADER. The baud rate R_s is 8 MSymbols/s. A Square Root Raised Cosine (SRRC) filter with a rolloff factor of 0.35 and an upsampling factor of 4 filters every frame. The value of the rolloff factor doesn't provide the best transmission capacity but minimizes the non-linear degradation by satellite in single carrier operation[3]. The summary for all simulation parameters is in Table 4.1.

Table 4.1: Simulation parameters.

Parameter	Value	Parameter	Value
Modulation	16 APSK	Carrier Frequency	12 GHz
Rs	8 MSymbols/s	SRRC Span	10 Samples
Upsampling factor	4 Samples/Symbol	SRRC rolloff factor	0.35
PLFRAME Type	Normal	NFFT for Coarse Frequency Estimation	2048
PLFRAME Length	32490 Symbols	NFFT for Fine Frequency Estimation	$2048 * 4$
SIR	0 dB		

4.3.3 Simulation Results

Firstly, we find the optimum FFT size that achieves the best performance under no frequency offset and noiseless conditions. Then, we evaluate the system performance in terms of BER for different SNR values under frequency offsets. Additionally, we find the RMSE of the estimated echo of the transmitted signal and the RMSE of its estimated frequency offset.

As the system performance depends on the accuracy of the estimated frequency offset, the frequency estimator should provide high frequency resolution. That accuracy varies with the size of the FFT operation employed in the estimation of the residual frequency offset. The following figures show the system performance at different FFT sizes, in ideal conditions, i.e. the absence of noise and under no frequency offset, for both transmitted and received signals. Intuitively, the system gives better performance when large FFT is used.

Figure 4.5 shows the BER of the received frames at different FFT lengths. It is clear from the figure that the FFT of size larger than $251K$ gives an error-free

output. The accuracy of the estimation of the transmitted signal echo and its frequency offset should be considered as well, to minimize the SI.
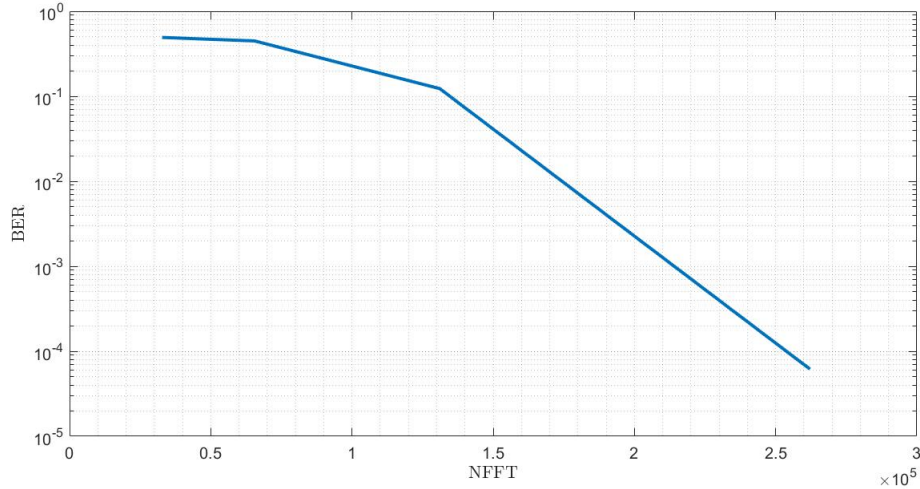

Figure 4.5: BER of the received frames vs NFFT of residual frequency offset estimation in ideal conditions.

Figure 4.6 and Figure 4.7 show the RMSE in estimated frequency offset for the echo of the transmitted frames at different FFT lengths and the RMSE in the estimated echo of the transmitted signal at different FFT lengths, respectively. From both figures, we can deduce that the suitable FFT size varies around 1 million-points. Although, this large FFT seems unfeasible in real time, the recent works in [57] and [58] break the large FFT bottlenecks in terms of hardware and speed.

The large FFT minimizes the inherited bias in non-linear discrete frequency estimation techniques. This bias tends to vanish when the FFT size increases significantly or the SNR becomes high enough[59]. Intuitively, large FFT gives a more accurate outcome by providing more frequency bins.
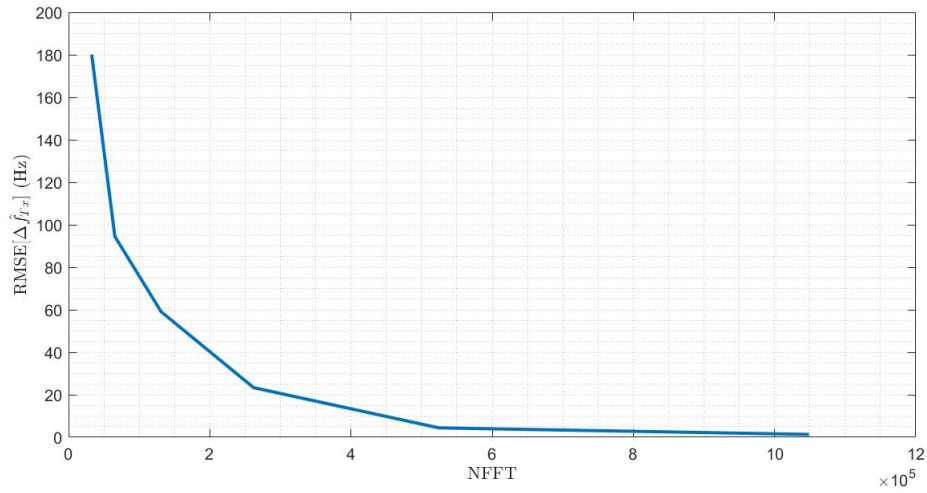
Figure 4.6: RMSE of estimated frequency offset in transmitted frame's echo vs NFFT of residual frequency offset estimation.
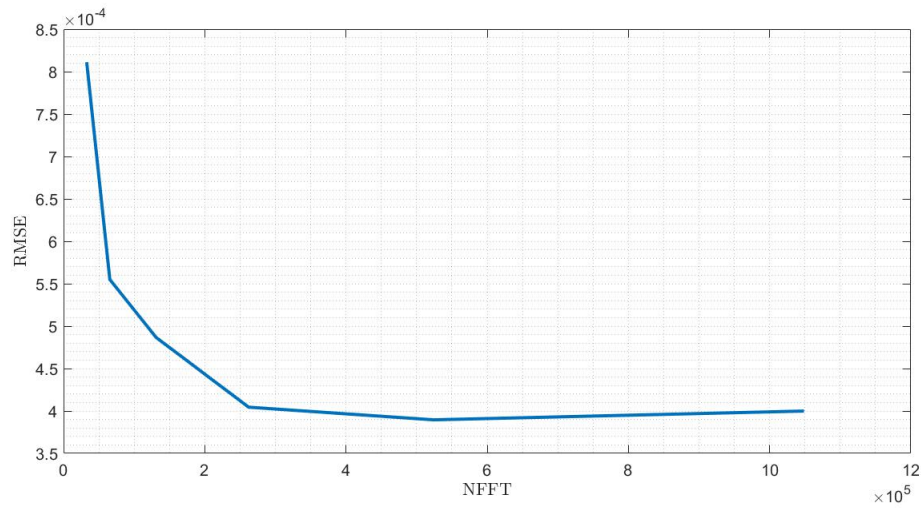

Figure 4.7: RMSE of the estimated echo of the transmitted frame vs NFFT of residual frequency offset estimation.

Figure 4.8 shows the BER for a scenario in which no frequency offset exists. The figure shows that the system operation requires an additional minimum SNR margin of around $2.5dB$ more than a conventional HD receiver, and have a minimum operating SNR of $10dB$, which is lower than the required SNR to

49

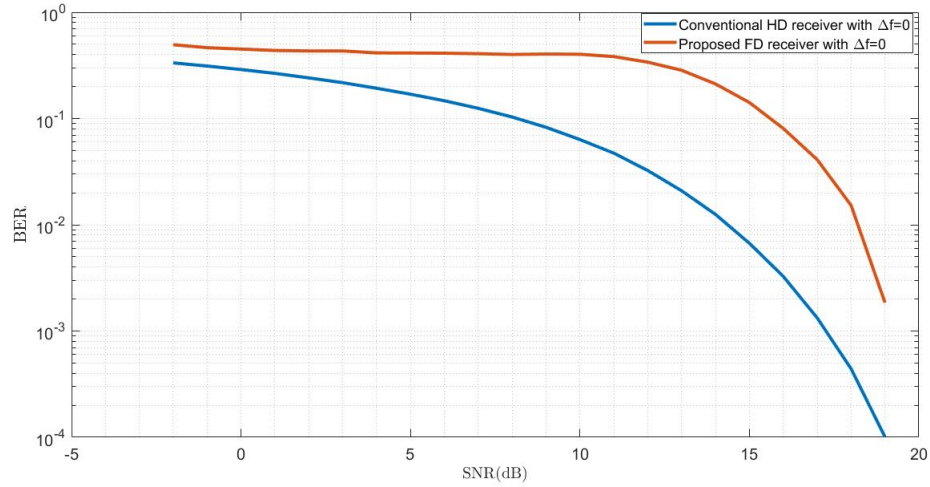achieve quasi-error-free Packet Error Rate (PER) for almost all 16APSK coding schemes[3].

Figure 4.8: Received frame BER vs SNR under no frequency offset.

The system performance for frequency offset of $-0.5Rs$ and $0.5Rs$ for transmitted and received frames respectively is shown in Figure 4.9. As the SNR increases, the additional required SNR margin to reach the same performance as a HD receiver decreases.
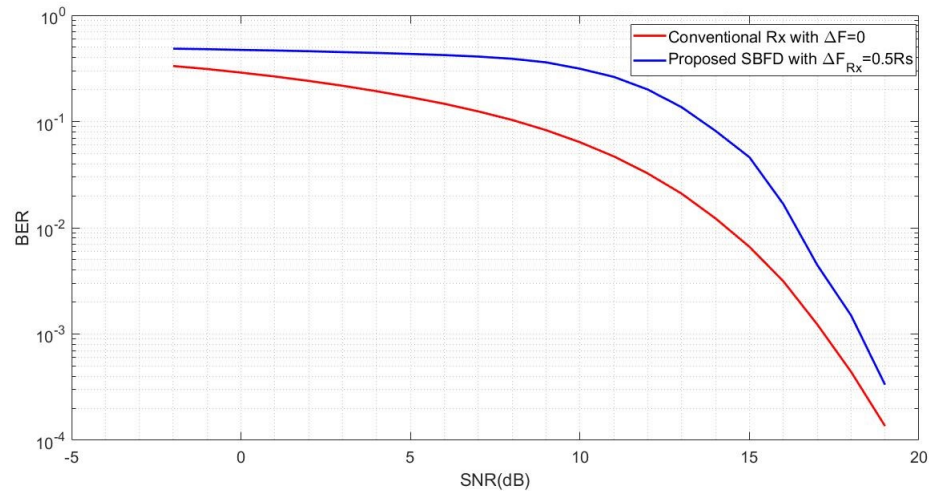

Figure 4.9: BER vs. SNR of different frequency offsets for transmitted and received frames.

Figure 4.10 shows the system performance compared to that of a conventional DVB-S2 receiver with no frequency offset. The transmitted and received frames in the superimposed signal have a frequency offset of $0.14Rs$, where Rs is the symbol rate.
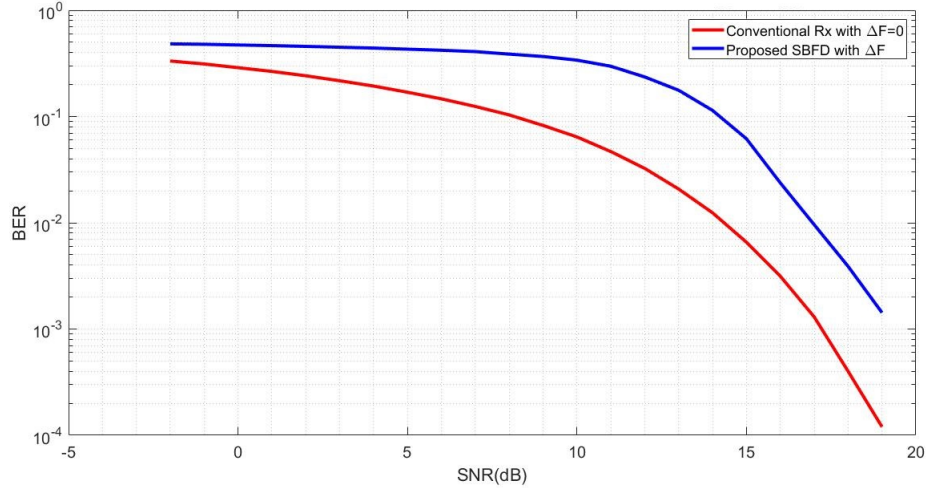

Figure 4.10: BER vs. SNR for frames with $\Delta f = 0.14Rs$ compared to frequency offset-free conventional DVB-S2 frames.

Figures 4.8, 4.9 and 4.10 show that the system gives better performance when the frequency offset of the received signal is different from that of the transmitted signal. If the the transmitted signal has the same frequency offset as the received signal, a larger additional SNR margin is needed to reach the same BER of a HD conventional receiver. This is valid even at high SNR. If both frequency offsets are different, the margin decreases at high SNR.

In both figures, it is clear that the BER is decreasing with the increase in SNR and the BER that a conventional DVB-S2 receiver achieves can be reached by increasing SNR. For a receiver operating in the range of SNR above 10 dB, the additional required SNR to achieve the same BER varies between 4 dB at SNR 10 dB and less than 1 dB at SNR 19 dB.

Figure 4.11 shows the RMSE of the frequency offset estimation of the transmitted frame's echo. The difference between the estimated frequency offset and

the real value doesn't exceed 40 Hz which is equivalent to $2.5^{-6}Rs$. This small offset has a negligible effect when estimating the echo of the transmitted signal. The error value can reach as low as almost 19 Hz. The value of error is not continuously decreasing with the SNR increase due to factors such as the low SIR value and the limited resolution of the FFT operation.
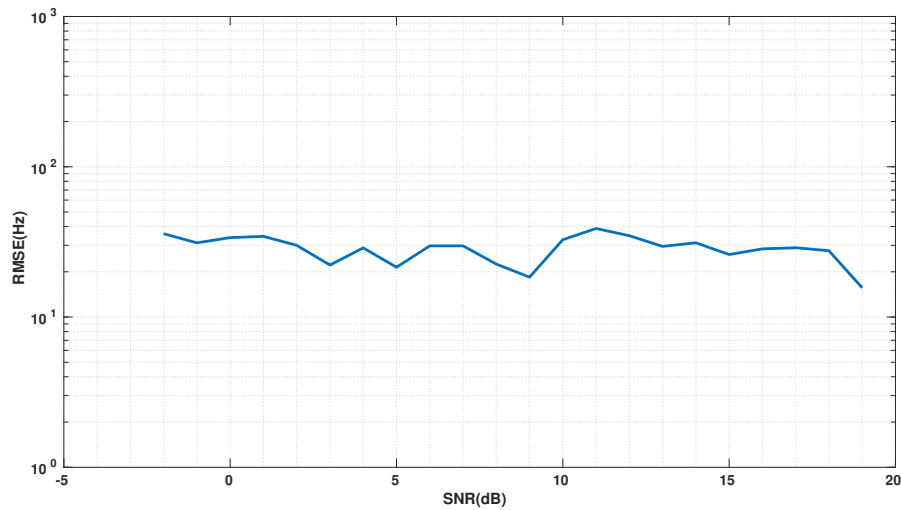

Figure 4.11: RMSE of the estimated frequency offset for the transmitted signal's echo.

Figure 4.12 shows the RMSE of the estimated echo of the transmitted signal. The RMSE value is very small within the shown range of SNR. The low RMSE value allows almost perfect SIC.
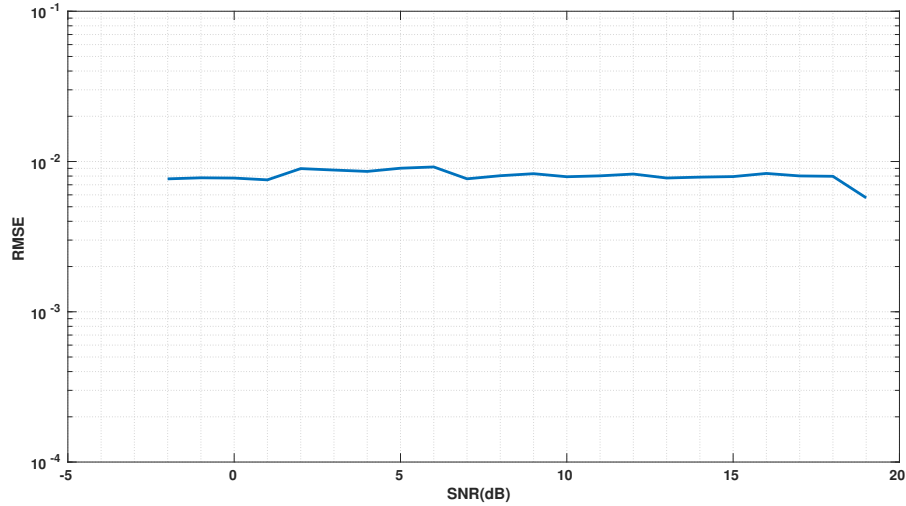
Figure 4.12: RMSE of the estimated echo of the transmitted signal.

4.4   Complexity Analysis

Firstly, we neglect the operations that are used in the transient state of the system, such as the early cross-correlations applied to find the frame edges. The system rely on that correlation for a limited time until it acquires the frames and becomes able to decode the frame length information and thus, identify the frames edges using the constant transmission feature.

Then, we find the number of arithmetic operations for every processing step in the proposed method. The complexity for the SIC and the synchronization of the received frame are shown in Table 4.2 and Table 4.3, respectively.

The complexity of every step is evaluated as the number of real additions R_A, real multiplications R_M and trigonometric functions T_{Func} employed. A T_{Func} itself can be expressed in terms of a number of R_As and R_Ms, but that number will vary according to the implementation.

The system complexity is a function of the frame length N and the number

of constellation points N_{const}, which affects the complexity of the DD phase synchronization step. The shown computational cost is the highest possible cost and better implementations can achieve the same performance with much lower complexity. Still, the bottleneck remains the FFT operation, which can be performed in real time using the means mentioned in [58], [60] and [57].

Step	Complexity
Apply $\Delta \hat{f}_{Tx,prior}$	$N(8R_M + 2R_A + 2T_{Func})$
Find MSE	$(2N + 1)R_M + (6N - 1)R_A$
Find $\Delta \hat{f}_{Tx,ML}$	$600.4 * 10^6 R_A + 400.3 * 10^6 R_M$
Compensate STx_{echo} by $\Delta \hat{f}_{Tx,prior} + \Delta \hat{f}_{Tx,ML}$	$8N.R_M + 2N.R_A + 2N.T_{Func}$
Find MSE	$(2N + 1)R_M + (6N - 1)R_A$
Find $Proj_{Tx(\Delta \hat{f}_{Tx})}S$	$2(N - 1)R_A + 4N.R_M$
Subtract $\hat{Tx}(\Delta \hat{f}_{Tx})$ from S	$2N.R_A$

Table 4.2: Complexity of SIC

Step	Complexity
S_{Rx} wavelet denoising	$(16R_M + 2R_A)(15N/8 + 12)$
Apply $\Delta \hat{f}_{Rx,prior}$	$2N(4R_M + R_A + T_{Func})$
Find MSE	$(2N + 1)R_M + (6N - 1)R_A$
Find $\Delta \hat{f}_{Rx,ML}$ using PLHEADER	$387 * 10^3 R_A + 258 * 10^3 R_M$
Find MSE	$(2N + 1)R_M + (6N - 1)R_A$
DD phase synchrnization	$T_{Func}(800 + 2 * N_{const}(N - 90)) +$ $+R_M(5720 - 2N + 15N_{const}(N - 90))$ $+R_A(3012 - N + 9N_{const}(N - 90))$

Table 4.3: Complexity of the received frame synchronization

4.5 Conclusion

In this chapter, we discussed the details of the proposed system. We evaluated its performance in BER and RMSE at different SNR values in multiple frequency offset scenarios. We showed that the system has the capability to estimate and cancel its echo with high accuracy.

Additionally, we investigated the size of the employed ML FFT operation in residual frequency estimation, and its effect on the the RMSE of the echo of the transmitted signal and the RMSE of its estimated frequency offset. Furthermore, we found the required FFT size to achieve error-free reception in ideal conditions.

Finally, the system showed a noticeable degradation in performance when the transmitted and received signal have similar frequency offsets. In this case, the system need higher additional SNR margin to achieve the same BER it could achieve if the frequency offset were different.

Chapter 5

Conclusion and Future Work

5.1   Conclusion

In this thesis, we proposed a digital SIC and synchronization algorithm for IBFD P2P satellite communication links, in which, a bent-pipe satellite acts as a relay. The DL from the satellite to a user has the user's transmitted message and its desired received message superimposed on the same spectrum bandwidth. Both earth users transceivers operate according to DVB-S2 standard. The proposed algorithm exploits the DVB-S2 features to maximize the capacity in non-pilot mode. The proposed algorithm cancels the SI and synchronizes the desired received signal by compensating for the carrier frequency offset using the preamble, while targeting the 16-APSK modulation option of DVB-S2.

In our work, we used conventional cross-correlation to find the frame edges and distinguish the transmitted signal from received one. We performed coarse and fine frequency synchronization for both messages using ML FFT estimator with the preamble. Wavelet denoising and decision-directed phase recovery were used for filtering the received signal and compensating for the residual phase offset, respectively. This work provides preliminary results of a substitute of DoubleTalk® patented technology, for systems employing DVB-S2 standard.

Matlab simulations showed that the system performance is comparable to the performance of the frequency offset-free conventional DVB-S2 receiver, in the cost of additional SNR. Few studies on DoubleTalk® system exist. These studies reveals the system performance after applying DVB-S2 error-correction. Thus, in our work, we compared the proposed system performance to that of an uncorrected HD DVB-S2 system.

5.2   Future Work

The conducted research herein provides a low-level implementation of IBFD satellite communications for DoubleTalk® CnC like systems. While the proposed work focuses on high order modulation of DVB-S2 in non-pilot mode, developing a similar system to achieve SIC independent of the standard is expected to have greater impact for systems supporting additional standards.

Additionally, employing machine learning techniques to develop a system that considers non-linear effects such as the IQ impairments and travelling wave tube modelling, is expected to create a system that can achieve the best performance and lowest complexity with high robustness against noise.

Nevertheless, as this work supports only 16-APSK, future research can lead to its generalization for higher order modulation, such as 32-APSK allowing for even higher capacity. A good addition to this work is to extend the proposed model to support schemes in DVB-S2 Extended (DVB-S2X) like 64/128/256 APSK.

Bibliography

[1] "Carrier-in-carrier technology," *Telesat*, July 2010.

[2] G. D. Collins and J. Treichler, "Practical insights on full-duplex personal wireless communications gained from operational experience in the satellite environment," in *2015 IEEE Signal Processing and Signal Processing Education Workshop (SP/SPE)*, pp. 136–141, 2015.

[3] "Digital video broadcasting (dvb); second generation framing structure, channel coding and modulation systems for broadcasting, interactive services, news gathering and other broadband satellite applications," european standard, European Telecommunications Standards Institute, France, 6 2006.

[4] Li Qing, Zeng Xiaoyang, Wu Chuan, Zhang Yulong, Deng Yunsong, and J. Han, "Optimal frame synchronization for dvb-s2," in *2008 IEEE International Symposium on Circuits and Systems*, pp. 956–959, 2008.

[5] E. Casini, R. D. Gaudenzi, and A. Ginesi, "DVB-S2 modem algorithms design and performance over typical satellite channels," *International Journal of Satellite Communications and Networking*, vol. 22, no. 3, pp. 281–318, 2004.

[6] A. B. Awoseyila, *Robust Synchronization for PSK (DVB-S2) and OFDM Systems.* PhD thesis, University of Surrey, Guildford, Surrey, GU2 7XH, UK, 2008.

[7] D. Rife and R. Boorstyn, "Single tone parameter estimation from discrete-time observations," *IEEE Transactions on Information Theory*, vol. 20, no. 5, pp. 591–598, 1974.

[8] O. Faust, U. R. Acharya, H. Adeli, and A. Adeli, "Wavelet-based eeg processing for computer-aided seizure detection and epilepsy diagnosis," *Seizure*, vol. 26, 01 2015.

[9] R. Polikar, "The wavelet tutorial second edition part i," *Indian Institute of Technology Delhi*.

[10] V. Smil, "Sputnik at 60 [numbers don't lie]," *IEEE Spectrum*, vol. 54, no. 10, pp. 20–20, 2017.

[11] G. W. Swenson, "Looking back: Sputnik," *IEEE Potentials*, vol. 16, no. 1, pp. 36–40, 1997.

[12] "Explorer-I and Jupiter-C," *Department of Astronautics, National Air and Space Museum, Smithsonian Institution*, Oct 2007.

[13] "Turkey candidate for ITU council region B - Western Europe," *Information and Communication Technology Authority*, 2018.

[14] "Extraordinary administrative radio conference to allocate frequency bands for space radiocommunication purposes (Geneva, 1963)," *Telecommunication Journal*, vol. 30, no. 12, pp. 366–368, 1963.

[15] "Space network list (SNL)," *ITU-R*, Dec 2004.

[16] D. Wood, "History of the DVB project ," 2013.

[17] E. Johnston, "Internet vsat access via satellite: costs," Feb 2005.

[18] K. E. Kolodziej, S. Yegnanarayanan, and B. T. Perry, "Fiber bragg grating delay lines for wideband self-interference cancellation," *IEEE Transactions on Microwave Theory and Techniques*, vol. 67, no. 10, pp. 4005–4014, 2019.

[19] A. "Nadh, R. Jagannath, Ganti, and R. Krishna", "TI - Self-interference cancellation in full-duplex wireless devices: A survey," *CSI Transactions on ICT*, vol. 7, pp. 3–12, 2019.

[20] S. Bojja Venkatakrishnan, E. A. Alwan, and J. L. Volakis, "Wideband RF self-interference cancellation circuit for phased array simultaneous transmit and receive systems," *IEEE Access*, vol. 6, pp. 3425–3432, 2018.

[21] M. G. M. Mark D. Dankberg, Mark J. Miller, "Self-interference cancellation for two-party relayed communication," U.S. Patent 5 596 439, Jan. 1997.

[22] M. J. R. Glenn D. Collins, Don L. Anair, "Adaptive canceller for frequency reuse systems," U.S. Patent 6 859 641 B2, Feb. 2005.

[23] M. J. R. Glenn D. Collins, Don L. Anair, "Adaptive canceller for frequency reuse systems," U.S. Patent 7 228 104 B2, Jun. 2007.

[24] S. McDermott and K. Irving, "The application of satellite communication technology to operational knowledge acquisition," in *MILCOM 2006 - 2006 IEEE Military Communications conference*, pp. 1–5, 2006.

[25] E. G. Tiedemann, "Channel access protocols for half duplex satellite terminals," in *IEEE Military Communications Conference, 'Bridging the Gap. Interoperability, Survivability, Security'*, pp. 463–469 vol.2, 1989.

[26] S. Lassandro, "Comtech EF data introduces new high-speed trunking modem that combines dvb-s2, acm & doubletalk carrier-in-carrier," *Comtech EF Data*, 2010.

[27] "Optimizing satellite communications using DoubleTalk Carrier-in-Carrier & CDM-625 advanced satellite modem," *Comtech EF Data*, Dec 2010.

[28] S. Chen, M. A. Beach, and J. P. McGeehan, "Division-free duplex for wireless applications," *Electronics Letters*, vol. 34, no. 2, pp. 147–148, 1998.

[29] M. R. Bhavani Shankar, Gan Zheng, S. Maleki, and B. Ottersten, "Feasibility study of full-duplex relaying in satellite networks," in *2015 IEEE 16th International Workshop on Signal Processing Advances in Wireless Communications (SPAWC)*, pp. 560–564, 2015.

[30] S. S. Bharj, B. Tomasic, J. Turtle, R. Turner, G. Scalzi, and S. Liu, "A full-duplex, multi-channel transmit/receive module for an s-band satellite

communications phased array," in *2010 IEEE International Symposium on Phased Array Systems and Technology*, pp. 202–210, 2010.

[31] E. Dahlman, S. Parkvall, and J. Sköld, *Chapter 24 - New 5G Radio-Access Technology*. Academic Press, third edition ed., 2016.

[32] Lu Tian, Shuai Wang, Zhiheng Cheng, and Xiangyuan Bu, "All-digital self-interference cancellation in zero-if full-duplex transceivers," *China Communications*, vol. 13, no. 11, pp. 27–34, 2016.

[33] E. Ahmed and A. M. Eltawil, "All-digital self-interference cancellation technique for full-duplex systems," *IEEE Transactions on Wireless Communications*, vol. 14, no. 7, pp. 3519–3532, 2015.

[34] D. H. Kong, H. Ju, and S. Kim, "On self-interference cancellation under the existence of desired signal in in-band full-duplex communications," in *2019 International Conference on Information and Communication Technology Convergence (ICTC)*, pp. 1002–1005, 2019.

[35] E. Türkyilmaz, "Development, implementation and assessment of DVB-S2 frame synchronization and SNR estimation on the GNU radio platform," Master's thesis, Graz University of Technology, Rechbauerstraße 12, 8010 GRAZ, AUSTRIA, 2012.

[36] K. K. Gupt, R. Bera, D. Bhaskar, P. Chettri, and D. Bose, "Smart home realization through wireless communication system," *viXra*, 2016.

[37] M. Renfors, "Tlt-5806 receiver architectures and signal processing, synchronization," *Tampere University of Technology*, 2012.

[38] A. Barbieri and G. Colavolpe, "On pilot-symbol-assisted carrier synchronization for dvb-s2 systems," *IEEE Transactions on Broadcasting*, vol. 53, no. 3, pp. 685–692, 2007.

[39] F.-W. Sun, Y. Jiang, and L.-N. Lee, "Frame synchronization and pilot structure for second generation dvb via satellites," *International Journal of Satellite Communications and Networking*, vol. 22, no. 3, pp. 319–339, 2004.

[40] Zae Yong Choi and Y. H. Lee, "Frame synchronization in the presence of frequency offset," *IEEE Transactions on Communications*, vol. 50, no. 7, pp. 1062–1065, 2002.

[41] B. Al-Qudsi, M. El-Shennawy, N. Joram, and F. Ellinger, "Crystal oscillator frequency offset compensation for accurate fmcw radar ranging," in *2016 German Microwave Conference (GeMiC)*, pp. 405–408, 2016.

[42] D. A. Emmons, D. W. Martin, and R. M. Garvey, "Satellite master oscillators," in *Proceedings of the 1995 IEEE International Frequency Control Symposium (49th Annual Symposium)*, pp. 600–613, 1995.

[43] A. Presser and J. Camparo, "Examination of a crystal oscillator's frequency fluctuations during the enhanced space-radiation environment of a solar flare," *Nuclear Science, IEEE Transactions on*, vol. 49, pp. 2605 – 2609, 11 2002.

[44] Y. S. Shmaliy, "Quartz crystal oscillator with an effective aging rate compensation," vol. 1998, March 1998.

[45] J. R. Vig, "Introduction to quartz frequency standards," technical report, U. S. ARMY LABORATORY COMMAND Electronics Technology and Devices Laboratory, Fort Monmouth, NJ 07703-560, 3 1992.

[46] J. R. Vig, C. Audoin, L. S. Cutler, M. M. Driscoll, E. P. EerNisse, R. L. Filler, R. M. Garvey, W. J. Riley, R. C. Smythe, and R. D. Weglein, "The effects of acceleration on precision frequency sources," technical report, U. S. ARMY LABORATORY COMMAND Electronics Technology and Devices Laboratory, Fort Monmouth, NJ 07703-560, 7 1992.

[47] M. Luise and R. Reggiannini, "Carrier frequency recovery in all-digital modems for burst-mode transmissions," *IEEE Transactions on Communications*, vol. 43, no. 2/3/4, pp. 1169–1178, 1995.

[48] U. Mengali and M. Morelli, "Data-aided frequency estimation for burst digital transmission," *IEEE Transactions on Communications*, vol. 45, no. 1, pp. 23–25, 1997.

[49] M. P. Fitz, "Planar filtered techniques for burst mode carrier synchronization," in *IEEE Global Telecommunications Conference GLOBECOM '91: Countdown to the New Millennium. Conference Record*, pp. 365–369 vol.1, 1991.

[50] U. Mengali, *Synchronization Techniques for Digital Receivers*, vol. 1. Springer US, 1997.

[51] C. B. Uvo, "Fourier and wavelets transforms." University Lecture.

[52] F. A. Tripta, S. B. A. Kumar, and T. C. S. Saha, "Wavelet decomposition based channel estimation and digital domain self-interference cancellation in in-band full-duplex ofdm systems," in *2019 URSI Asia-Pacific Radio Science Conference (AP-RASC)*, pp. 1–4, 2019.

[53] A. Phinyomark, P. Phukpattaranont, and C. Limsakul, *The Usefulness of Wavelet Transform to Reduce Noise in the SEMG Signal*, pp. 107–132. 01 2012.

[54] "Digital satellite broadcasting system with flexible configuration (television, sound and data)," ITU-R satellite delivery, International Telecommunication Union - Recommendation Sector, Geneva, Dec 2016.

[55] S. Jung, J. G. Ryu, D.-G. Oh, and H. Yu, "Self-interference cancellation for shared band transmission in nonlinear satellite communication channels," *ETRI Journal*, vol. 39, no. 6, pp. 771–781, 2017.

[56] S. Jung and D.-G. Oh, "Frequency estimation for non-pilot mode of dvb-s2 system," *Proceedings of the World Congress on Engineering and Computer Science*, vol. 1, 2012.

[57] H. Kanders, T. Mellqvist, M. Garrido, K. Palmkvist, and O. Gustafsson, "A 1 million-point fft on a single fpga," *IEEE Transactions on Circuits and Systems I: Regular Papers*, vol. 66, no. 10, pp. 3863–3873, 2019.

[58] G. Xing and Z. Yao, "Real time recursive very large fft on multicore dsp platforms," in *2019 12th International Congress on Image and Signal Processing, BioMedical Engineering and Informatics (CISP-BMEI)*, pp. 1–5, 2019.

[59] C. Candan, "A method for fine resolution frequency estimation from three dft samples," *IEEE Signal Processing Letters*, vol. 18, no. 6, pp. 351–354, 2011.

[60] F. Han, L. Li, K. Wang, F. Feng, H. Pan, B. Zhang, G. He, and J. Lin, "An ultra-long fft architecture implemented in a reconfigurable application specified processor," *IEICE Electronics Express*, vol. 13, 06 2016.

SOFTWARE IMPLEMENTATION OF KEY TRANSCEIVER ALGORITHMS FOR AN IN-BAND FULL-DUPLEX DVB-S2-BASED SATELLITE COMMUNICATION SYSTEM